Development of Non-invasive Procedure for Evaluating Absolute Intracranial Pressure Based on Finite Element Modeling

by

Zhaoxia Li

A Thesis submitted to the Faculty of Graduate Studies of

The University of Manitoba

in Partial Fulfilment of the Requirements for the Degree of

Master of Science

Department of Mechanical and Manufacturing Engineering

Faculty of Engineering

University of Manitoba

Winnipeg, Manitoba

August 2010

Abstract

Elevated intracranial pressure (ICP) in closed head injury may lead to a vegetative state and even death. Current methods available for measuring ICP may cause infection, haemorrhage or not reliable. A patient-specific correlation between ICP and an external vibration response was used for ICP evaluation, which based on finite element (FE) modeling. In FE modeling, a two dimensional FE model of human head was built in ANSYS. Geometry information was obtained from a magnetic resonance image of the human head, while the material properties were acquired from literatures. Vibration responses, e.g., displacement, velocity, acceleration and equivalent strain, were obtained for applied ICPs in FE analyses. Correlations between ICP and vibration responses were established. Effects of impact magnitude and impact duration were studied. Response sensitivity was defined to find a vibration response that is sensitive to ICP change. A procedure based on response sensitivity was proposed for ICP evaluation.

Acknowledgments

I would like to begin by giving sincere gratitude to my supervisor, Dr. Yunhua Luo, for his excellent guidance and invaluable support on improving my learning and research ability. Thanks for his meticulous help on non-academic aspects which enables me over-coming difficulties in my life, and further for his exceptional direction in building right perception and understanding about study, work and life.

Genuine appreciation is presented to my co-advisor, Dr. Qiang Zhang, for providing me the opportunity and partial financial aid to study in Canada, and for offering me the chance to transfer to Mechanical and Manufacturing Engineering Department, which will influence my future career considerably. Moreover, thanks for his guidance in my thesis.

Great thanks rendered to Dr. Q. Peng, Dr. M. Xing, Dr. Z.K. Moussavi, Dr. D.B. Levin, Dr. G. Crow, Dr. Q.C. Wu and Dr. N. Sepehri for their guidance and teaching in my courses.

I want to express my sincere thanks to all of my friends for their care, encouragement and support. Special thanks bestowed to Wen Tan.

As always, I am grateful to my family who have supported me along the way.

Finally, it is gratefully acknowledged that the research reported in this thesis was partially supported by Manitoba Medical Service Foundation.

Dedicated to my deeply loved mom

母亲, 人间第一亲;

母爱, 人间第一情.

-献给我深爱的母亲

Contents

List of Tables

List of Figures

Nomenclature

Symbols:

c	Sound speed
i	Index: $i = 1, 2$ and 3
l	Length
p	Pressure
u	Displacement vector
t	Time variable
σ	Vector containing stress components
μ	Matrix containing damping coefficients of the solid materials
ρ	Mass density of a material
n	Normal to a solid-fluid interface
v	Velocity
$\emptyset$	Field function
Δt	Time step
v	Poisson's ratio
ψ	Sensitivity
ω	A vibration response

Δ	Increment
∇	Differentiation operator
D	Material property matrix
J	Jacobian matrix
F	Force vector
K	Elastic bulk modulus
L	Triangular matrix
Q	Fluid-solid coupling matrix
S	Fluid-solid interface
u, v	Displacement in x, y direction, respectively
ξ, η	Natural coordinates
β, γ	Integration parameters
x, y, z	Physical coordinates

Symbols with superscript or subscript:

C^s	Damping matrices
K^s	Stiffness matrices
M^s	Mass matrices
B_s	Strain-displacement matrix
F_0	Magnitude of impact force
N_i	Shape functions: $i = 1, 2, 3, 4$
N_u	Shape functions of element displacements

N_{p}	Shape functions of element pressure
Ω_{s}	Domain of solid part
Ω_{f}	Domain of fluid part
ρ_{s}	Density of solid part
ρ_0	Hydrostatic density of the cerebrospinal fluid
t_0	Impact duration
ε_{e}	Equivalent strain
τ_{xy}	Shear stress in xy plane
$\mu_{\mathrm{x}},\ \mu_{\mathrm{y}}$	Damping coefficients in *x*, *y* direction, respectively
ω_u, ω_l	Upper and lower value of a vibration response, respectively
$\sigma_{\mathrm{x}}, \sigma_{\mathrm{y}}, \sigma_{\mathrm{z}}$	Normal stress in *x*, *y*, *z* direction, respectively
$\widetilde{(\,)}$	Discrete value of a variable at element nodes
$\dot{(\,)}$	First derivate of a variable with respect to time
$\ddot{(\,)}$	Second derivate of a variable with respect to time
$\dddot{(\,)}$	Third derivate of a variable with respect to time
$\overline{(\,)}$	Effective variable matrix or vector
$(\,)^T$	Transpose of a vector or matrix
$(\,)_a$	Averaged value of a variable
$(\,)_x$	Vibration response in *x* direction

Abbreviations:

2D	Two-dimensional
3D	Three-dimensional
CBF	Cerebral blood flow
CHI	Closed head injury
CPP	Cerebral perfusion pressure
CSF	Cerebrospinal fluid
CT	Computed tomography
FE	Finite element
ICP	Intracranial pressure
LS	Loading step
MBF	Mean blood pressure
MR	Magnetic resonance
MRI	Magnetic resonance imaging

Chapter 1

Introduction

Head injury in human is a major cause of fatality in different age groups all over the world even various protective devices have been adopted [1]. Incidents of head injury occur in traffic accidents, sports, violence, construction, falls, recreation and some other situations [2, 3]. Based on second-injury status of skull bone, head injuries are roughly classified as open head injury, or penetrating head injury, and closed head injury (CHI), or non-penetrating head injury [4, 5]. For an open head injury, an object hits the head and the object breaks the skull and penetrates into the brain. Sharp objects (e.g., a knife) and small objects of high velocity (e.g., a gunshot) usually cause the injuries [6]. Indications of open head injury are obvious, e.g., bleeding and skull fracture. Therefore, open head injury patient usually receives immediate attention and timely treatment. CHI usually results from rapid acceleration or deceleration, with or without external impact, and most often occurs in traffic accidents and falls [7, 8, 9]. In closed head injuries, the interaction force between skull and brain does not lead to skull fracture, but it damages the brain or causes haemorrhage. External signs of CHI, like slightly geometry changes of

human head, are much less obvious than those of open head injury. Therefore, it is difficult to detect and treat CHI in time. Intracranial pressure (ICP) is a paramount parameter that reflects the severity and physiological state of a CHI patient. Timely ICP evaluation of a CHI patient is crucial to prevent permanent disability and death. To better understand the ICP effects on closed head injury, Section 1.1 introduces ICP and its characteristics. In Section 1.2, the current available methods for measuring and monitoring ICP are reviewed. Objective and outline of the thesis are described in Section 1.3 and Section 1.4, respectively.

1.1 Intracranial pressure and its characteristics

Intracranial pressure has long been recognized as a significant observation indicator in clinics and in research for Neurosurgery. Information and parameters derived from ICP provides direct insight into the pathophysiology of the impaired brain, and waveform of ICP offers valuable information about impending trends in CHI patient [10].

1.1.1 ICP and closed head injury

To make the understanding of ICP definition and the mechanism of CHI better, the anatomical structure of human head is analyzed here. Fig.1.1 shows an anatomical cross-section of human head. From the outermost layer to the innermost layer, there mainly are scalp, skull, dura mater, superior sagittal sinus and brain. The skull is composed of cranium and mandible. The volume space that is enclosed by the skull which mainly contains brain, cerebrospinal fluid (CSF) and blood are considered fixed [10]. Cerebrum,

corpus callosum, thalamus, pons and cerebellum are the main components of brain, and they are labeled in Fig. 1.1. Intracranial pressure is the pressure exerted on the brain's intracranial blood circulation vessels and it could be regarded as the environmental pressure in the cranium [10, 11, 12, 13]. Volumes of brain, CSF and blood are the main factors influencing ICP. The Monro-Kellie doctrine dictates the pressure-volume relationship between ICP, volume of CSF, blood and brain [14]. The Monro-Kellie hypothesis states that the constituents within the cranium compartment which mainly are brain, CSF and blood are maintained in a state of volume equilibrium, meaning that any increase in the volume of one cranial constituent must be compensated by a volume decrease of the others [14]. CSF and blood volume are the main buffers for volume increase of the brain. For instance, an increase in lesion volume occurring in epidural hematoma is compensated by the decrease of CSF and venous blood [14]. In a healthy human, volume changes in one intracranial constituent that could be compensated by others is less than 120 ml (the value may vary slightly with different people) [14]. The volume changes which could not be compensated would lead to ICP change.

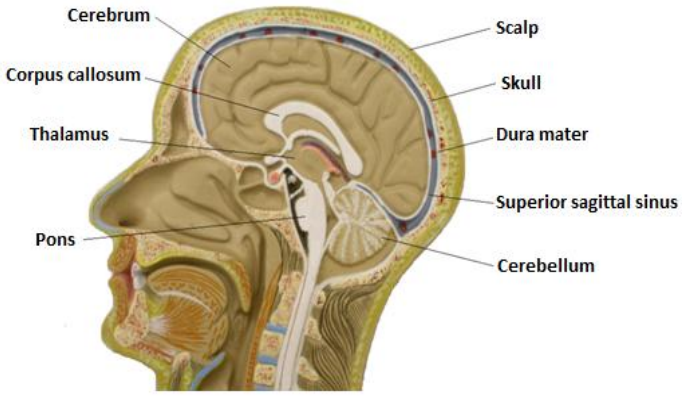

Figure 1.1: Anatomical structure of the human head (sagittal plane)
(Modified from Human-Anatomy.com)

1.1 Intracranial pressure and its characteristics

In human head, brain is protected by some components, such as the skull, the CSF, the meninges and the blood brain barrier. The main function of skull is to protect the brain from penetrating injuries. From the point view of mechanics, the CSF acts as a cushion to protect the brain from an impact. The skull and the CSF may be also considered as damping materials and they absorb a certain amount of kinetic energy induced by an impact [4]. To some extent, the meninges, layers of tissue that separate the skull and the brain, can further attenuate kinetic energy induced in an impact. Although the hard skull can effectively protect the brain against penetration, it cannot completely prevent kinetic energy from the impact to reach the brain [4]. Under an impact, the motion of the brain will lag behind that of the skull due to mechanical property differences between the skull and the brain [4, 15]. This type of relative motion produces dynamic strains and stresses in the brain, and excessive stresses or strains will damage the brain blood vessels and result in intracranial bleeding and causes CHI [4]. A helmet is similar to the skull to prevent brain from injury. That is, a helmet hinders direct impact to the head from external object, but it cannot completely eliminate kinetic energy of the impact transmitted to the skull and then to the brain. Therefore, helmets cannot effectively prevent the relative motion between the skull and the brain, which may lead to a CHI. This may explain why helmets and some protective apparatus are effective to prevent open head injuries, but have less effect in preventing closed head injuries.

Intracranial bleeding in CHI will lead to elevated ICP. The mechanical mechanism is described in the following. Adopting Monro-Kellie hypothesis, human skull is considered as a shell-like container which is very rigid and the enclosed volume is fixed. The base for the hypothesis is that the bones of the skull have much higher Young's modulus than

that of brain and other intracranial constituents [15, 16, 17]. Therefore, the enclosed volume by the skull would not increase correspondingly when the skull is overfilled with internal bleeding and swollen brain tissue. Without corresponding skull enclosed volume change, the pressure inside the skull would be elevated. That is the elevated ICP. The more internal bleeding and swollen brain tissue, the more volume change of the intracranial constituents, and the higher ICP.

1.1.2 Importance of monitoring ICP in closed head injury

The physiological importance of ICP lies in its effect on cerebral perfusion pressure (CPP) and its influence on stable cerebral blood flow (CBF) [10]. CPP is the net pressure gradient causing blood flow to the brain (i.e., brain perfusion), and stable CBF is the normal amount of blood supply to the brain in a given time. If a patient has an elevated ICP, the CPP will be lower than that of a normal person for the given level of mean blood pressure (MBF) (CPP=MBF-ICP) [18]. However, in undamaged brain, mechanisms exist to maintain an adequate and stable CBF despite a wide range of CPP. This phenomenon is known as auto-regulation [18]. However, auto-regulation only works over a limited range of CPP. The CPP in severe closed head injury is out of the work range of auto-regulation mechanism. Fig.1.2 shows that CBF is approximately linearly dependent on CPP if auto-regulation fails to work. The failure of auto-regulation causes progressive reductions of CBF and leads to ICP's elevation. In other words, elevated ICP indicates the failure of auto-regulation. Once ICP rises to the mean blood pressure, stable cerebral blood flow cannot be maintained, and the brain dies [19]. Apparently, a CHI will be worsened by

elevated ICP. Hence, ICP evaluation provides us significant information about the severity of closed head injuries.

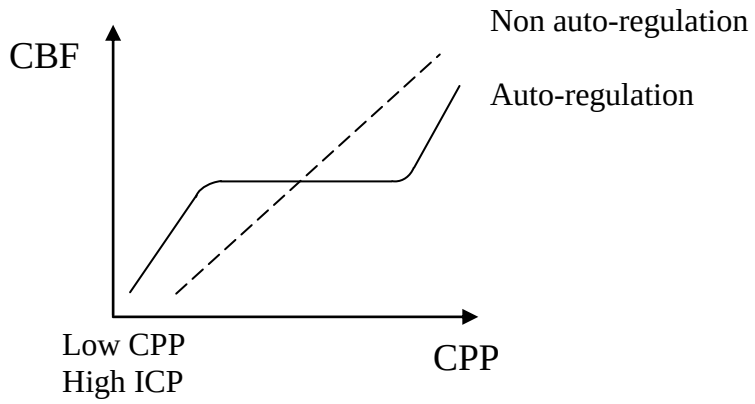

Figure1.2: Effect of cerebral perfusion pressure on cerebral blood flow

CBF= cerebral blood flow, CPP= cerebral perfusion pressure;
(Adopted from *Management of head injuries* by B. Jennett and G. Teasdale, 1981, F.A.Davis, Philadelphia.)

1.1.3 Normal range of intracranial pressure

Up to date, a universal "normal value" for ICP does not exist for all age groups. ICP is fluctuant owing to cardiac impulse, body position and breathing [20, 21, 22]. The normal range of ICP obtained from different investigators is different. Mick measured the normal range of ICP is 0 ~ 4 millimetres of mercury (mm Hg) and it becomes a concern when it reaches 20 mm Hg [22]. It is considered life threatening when ICP reaches 25 mm Hg for more than 2 minutes [22]. The normal range of ICP obtained by Merrit is 3 ~ 15 mm Hg [23]. Paraicz pointed out that for older children and adults, ICP value less than 15 mmHg

is considered as normal, exceeds 20 mmHg are unequivocally high, and ICP greater than 40 mmHg are considered as a severe condition [12, 24].

The normal value of ICP obtained by different investigators is different due to the following possible reasons. First, physical difference exists among the tested people. Even all the subjects are in the same age and all are in normal conditions, their physical differences may lead to different ICPs. Second, the methods used by the investigators are different. The methods employed are lumbar acupuncture, skull puncture, using ultrasound cephalohemometer, etc. Third, age is another major factor affecting ICP. There is a gradual increase in the normal ICP from birth through childhood with values of approximately 2 mmHg in the newborn, up to 5 mmHg by the end of infancy, and between 6 and 13 mmHg for the child up to 7 years old [12, 24]. The last but not the least reason is the body posture [25]. In a horizontal position, the normal ICP in healthy adult subjects was reported to be within the range of 7 ~ 15 mmHg [21, 25, 26]. In a vertical position, it is negative with a mean value around -10 mm Hg, but not lower than -15 mm Hg [25, 26, 27]. A change in the position of head or neck may significantly alter the cerebral venous blood volume and thus the ICP [20, 28, 29].

1.1.4 Elevated intracranial pressure

Elevated ICP, namely, exceeds the normal ICP range. Elevated ICP is a primary cause of irreversible brain damage [30]. When ICP exceeds its normal range, the brain may damaged by excessive mechanical stresses. If ICP reaches 30 mm Hg, venous drainage is impeded and edema develops in uninjured brain tissue which leads to ICP increases in turn

[19]. Sufficiently high ICP may lead to intracranial haematoma or cerebral edema, shift brain, displace brain stem, compress brain tissue and restrict blood supply to the brain [31]. Brain tissue is quite fragile since it consists of a complex network of neurons and blood vessels interspersed within a matrix of supporting cells [32], and an elevated ICP would crush it. Delayed treatment of high ICP may lead to permanent disability and even death [30].

1.2 Existing methods for monitoring or measuring ICP

Since there is no obvious external indication of CHI, and the human head has complex structure and complicated cranial contents, it is difficult to detect the physiological state of a CHI patient. Fortunately, advanced medical imaging technologies, such as magnetic resonance imaging (MRI), computed tomography (CT) and ultrasonic imaging techniques make the understanding of CHI much better than before [33, 34, 35, 36, 37]. However, medical images cannot reveal the injury severity quantitatively; it can only reflect the injury condition roughly. Measuring ICP is a significant way to detect patient's physiologic state and assess the effectiveness of a therapy to the patient [38].

Methods ranged from pressure sensor to ultrasonic technique have been developed for measuring or monitoring ICP. The methods can be either classified as invasive or non-invasive. Implanting a tiny sensor in the cranium or connecting an inserted needle to a monometer externally are two typical invasive ways [20, 28, 29]. For non-invasive methods, there are many ways have been explored for ICP determination with different bases.

1.2 Existing methods for monitoring or measuring ICP

For example, strain measurement, ultrasonic technology, acoustic property analysis, etc. In this section, several representative and commonly used methods for monitoring or measuring ICP are discussed.

1.2.1 Invasive methods

The main idea of an invasive method is producing a direct access to intracranial pressure. Typical sites for invasive measurement of ICP are lateral ventricles [39], extradural space and subdural or subarachnoid space [20]. Lumbar acupuncture, skull puncture, using ventricular catheter (for adults), and making use of tonometry are common invasive methods [20, 24, 40, 41]. In this article, lumbar acupuncture and skull puncture are discussed. Lumbar acupuncture is good for intermittent measuring, while skull puncture is preferred for continuous monitoring.

Lumbar acupuncture is a method to measure the pressure of CSF by an open-ended manometer [20, 24]. It is probably the first technique used as a clinical tool to measure ICP [20, 42]. In the spinal canal, free communication occurs between the spinal and cranial compartments, and thus the measured CSF pressure reflects the ICP [24]. For the intimate relationship between ICP and CSF, lumbar acupuncture is generally accepted as a method for measuring ICP. During a lumbar acupuncture operation, patient's position is extremely important. There are two commonly adopted positions. One is that the patient lies on a bed on one side with his knees drawn up toward his chest. The other one is that the patient sits on the edge of a bed or chair with his head and chest bent toward his knees. In both of these positions, the space between the lower spine bones is widened, and a

long and thin needle can be easily inserted into the spinal canal. When the needle is in place, a small amount of CSF will drop from the needle. Then, a manometer is attached to the needle to measure CSF pressure. For lumbar acupuncture, an accurate measurement of CSF pressure relies on the right position and adequate relaxation of the patient [40]. Under the guidance of a doctor, the patient may keep a right position for the measurement. Nevertheless, a relaxation status may not easy to achieve. A major drawback of this method is that sequelae may exist after the measurement. Headache is quite common following a lumbar acupuncture [43, 44]. Complications, like Bleeding in the spinal canal, damage to the spinal cord (particularly if the patient moves during the test) and subdural hematomas may occur in lumbar acupuncture.

Due to ICP is fluctuant, continuous monitoring of ICP is obviously more helpful, especially when the patient is in a severe condition. Skull puncture is a method that could be used for continuously monitoring ICP. In skull puncture, a hole is first punctured in the skull and a transducer which is small in size and sensitive to pressure change is then inserted into the skull through the hole [20, 28]. By the transducer, ICP is detected and displayed or recorded by an instrument. The transducer adopted could base on different physical principles [20]. For example, a pressure sensitive capsule (regarded as a form of transducer here) is either fluid or gas-filled. When the capsule is put in the cranium, it is pressed by ICP and the ICP is transformed into a hydraulic or gas pressure in the capsule. Then the hydraulic or gas pressure is measured by an external connected instrument. Strain gauge diaphragm is based on another physical principal. A strain will be produced in the diaphragm when a pressure is acting on it. Based on mechanics of material strength,

the strain magnitude is proportional to the magnitude of the pressure. In other words, the strain magnitude reflects the ICP.

Invasive methods are normally reliable for measuring an absolute or specific ICP, not for determining a relative or increased ICP. The main drawback of invasive methods is the risk of infection, and haemorrhage may occur. Owing to these, invasive methods are usually not adopted for susceptible cases of closed head injury.

1.2.2 Non-invasive methods

To date, a variety of non-invasive methods are available for measuring ICP. The main idea of a non-invasive method is to detect an externally measurable change, or second change, caused by ICP change. For instance, an elevated ICP may change the travel velocity of a sound wave in the head. Another example is that the perimeter of the head may have a small change under an elevated ICP. By measuring perimeter change, the change of ICP can be evaluated. Generally speaking, non-invasive methods are indirect, which may introduce uncertainties and inaccuracy, as they involve the solution of an inverse problem. One exception is the methods based on the palpation of the anterior fontanelle [45, 46]. ICP relates directly with the open scale of neonate's fontanelle. However, the methods are not applicable to older children and adults.

ICP changes may affect the acoustic properties of brain tissue and cranium, dura matter thickness, blood flow, parameters of an optic nerve, vessels of the eye, properties of skull bones, dynamic response of cerebral ventricle, etc. [30, 47, 48, 49, 50, 51, 52, 53,

54, 55, 56, 57, 58, 59, 60]. In the following, three methods that make use of vibrations and acoustics are discussed.

Elevated ICP causes the thickness change of dura mater. Although the changes are very small, they may still be measured by advanced technologies. One method is developed based on this fact. An ultrasonic cephalohemometer which contains an electrocardiograph, a pulser, an ultrasonic probe, a receiver and a processor [53] is used in the method. The processor includes an A/D converter and an arithmetic unit. The electrocardiograph is used to detect the heart beat of the patient. The pulser triggered by heart beat generates a voltage pulse which was converted into an ultrasonic wave pulse by the ultrasonic probe, and it is detected by the electrocardiograph. The receiver picks up the ultrasonic wave pulse which transverse into the cranium and the reflection waves. The processor processes the output from the receiver. By the A/D converter and the arithmetic unit, the thickness of the dura mater can be calculated. Finally, by comparing the calculated dura mater thickness with a reference value, dura mater thickness change is then obtained. The reference value refers to the dura mater thickness when people have normal ICP. Utilizing the correlation between ICP variation and dura mater thickness variation, the increased ICP can be evaluated in reference to the dura mater thickness change [53]. One problem in this method is that the reference value of dura mater thickness varies from individual to individual.

Making use of acoustic wave properties is another common non-invasive method. The acoustic wave properties, such as sound velocity, acoustic transmission impedance and resonance frequency are all relate to the ICP [50, 55, 58]. Take acoustic wave travel velocity as an example. ICP affects the travel velocity of acoustic waves in the cranium

by itself; the higher the ICP, the larger the velocity [50, 55, 58]. In addition, elevated ICP slightly changes the mass density of cranium parenchyma, which in turn influences acoustic wave velocity. Therefore, change in the acoustic wave travel velocity in the human head provides indication of elevated ICP. One non-invasive method based on using acoustic wave properties is Bridger's method, which is briefly described as follows [50].

Two acoustic signal transmitters are mounted at the two temples of human head, and one acoustic signal receiver is mounted at the forehead. Electronic signals which generated by a signal analyzer and amplified by an power amplifier are sent to the acoustic signal transmitters. Driven by the electronic signals, the acoustic signal transmitters generates acoustic waves. After traveling through the head, the acoustic waves are picked up by the receiver. Elevated ICP is indicated by the attenuation of the acoustic signals. Other indications of elevated ICP are shift in frequency, reduction or elimination of resonance peaks or new peaks in the signal patterns. Some drawbacks exist in this method. First, the externally mounted receiver, sensor, transmitter and amplifier may be affected by the environment noise. Therefore, the received signal may have a poor signal-to-noise ratio. Second, the characteristics of the measured acoustic signal are only correlated to changes in ICP [22], no explicit relation is available.

Dynamic vibration characteristics and behaviour such as natural frequency, mechanical impedance and frequency response spectrum of the skull bone are in relation with the stress status in the skull, which in turn is affected by ICP [42], Mick designed a non-invasive method for evaluating ICP [22]. In the method, a mechanical oscillation is applied to the skull, a mechanical wave is thus generated and transmits through the skull

non-invasively. The frequency response spectrum of the skull at a location can be measured and then used to evaluate the current ICP. In order to get a reference or normal value of the ICP, the frequency response spectrum at a point on the skull which is believed not affected by ICP is also measured. The locations considered not affected by ICP are temporal, sphenoid, lower portions of the occipital and lower parietal bones [22]. When comparing the ICP obtained from two locations, one is affected by ICP and the other is not affected, the changes in ICP can be therefore obtained. The problem in this method is that the reference ICP measured from the location which is believed not affected by ICP is inaccurate. Moreover, natural frequencies and frequency response spectrums of the skull bones may be different due to age, gender, race, etc. Therefore, Mick's method is appropriate for estimating ICP rather than obtaining ICP value.

Since existing non-invasive methods have many shortcomings, it is expected to find a new method to overcome those inadequacies. It has been found in previous experimental studies [61, 62, 63] that elevated ICP causes an external vibration response changes of an animal head. Moreover, a theory called initial stress theory makes a basis for establishing the correlation. The initial stress theory applied here is that an ICP produces initial stress fields in the skull, which in turn introduces a stress-related term in the skull stiffness. On the other hand, external vibration responses of human head relate to the skull stiffness. According to the above two points, it is not difficult to conclude that stiffness of the skull bridges ICP and the external vibration responses of human head. The finding and the theory above indicate that the possibility of establishing a correlation between ICP and an external vibration response of human head exists. Hence, finding the correlation between

ICP and vibration responses of the head is the first step for developing a non-invasive procedure for evaluating ICP.

1.3 Objective of the thesis

There are two major objectives of the research reported in this thesis:

1) To establish correlations between ICP and external vibration responses of human head. This includes building a 2D FE model, conducting FE analyses, collecting external vibration responses (e.g., displacement, velocity, acceleration and equivalent strain) and analyzing data.
2) To develop a non-invasive procedure for absolute ICP evaluation. This includes determination of a response that is very sensitive to ICP change, physical setup of the measuring instrument, and ICP evaluation by using established patient-specific correlation between ICP and an external vibration response.

1.4 Outline of the thesis

The rest part of this thesis is organized as follows. In Chapter 2, a two-dimensional (2D) finite element (FE) model of the human head will be built. First, a geometric model of human head, which constructed from a magnetic resonance image, will be introduced. Material properties of different components in human head are going to be introduced for afterwards material representation in the FE Modeling. This followed by describing governing equations and FE equations. The Newmark method will be introduced for solving the FE equations. The process for establishing the 2D human head FE model in ANSYS

will be described in the last section.

In Chapter 3, FE study of correlations between ICP and external vibration responses is conducted. Correlations between ICP and external vibration responses are explored in the first section of the chapter. Then, effects of two factors, the magnitude of applied impact and the duration of applied impact, on the correlations are studied and discussed.

In Chapter 4, response sensitivity will be defined to find a response sensitive to ICP change. A non-invasive procedure for evaluating ICP will be proposed based on the patient-specific correlations between ICP and an external vibration response of human head which is established in the FE modeling.

In Chapter 5, conclusions are made and future work is described.

Chapter 2

2D Finite Element Model of Human Head

Building a faithful patient-specific biomechanical model is vital for establishing correlations between ICP and vibration responses. Three types of biomechanical models are usually used to analyze human head responses to impact or inertial loading [64]. They are lumped parameter models, analytical continuum models and finite element models. Due to their inherent discrete nature, the main limitation of lumped parameter models is that they cannot describe the distribution of field parameters such as stress, strain and pressure in the model [64]. With analytical continuum models, field parameter distributions can be obtained. However, only with simple geometry, constitutive properties and boundary conditions, governing equations of analytical continuum models are solvable [64]. In FE method, a complicated differential equation which governing a problem is represented by a set of simple algebraic equations, and the solution to the differential equation is easy to get since the algebraic equations can be easily solved. FE modeling can handle very

complex geometries, complicated material composition and different kinds of non-linearity problems; it is recognized as a powerful and handy tool for exploring and analyzing many different aspects of the mechanical behaviour of human head under impact or inertial loading [64]. Due to the above reasons, FE method was employed in this study.

The basic idea of a FE method is that a given domain is viewed as a collection of sub-domains (called finite elements), and the governing equation is approximated by a traditional variational method, such as Galerkin method, collocation method and least-squares method [65]. Implementation of conducting a FE method includes pre-processing, solution and post-processing. ANSYS, an engineering simulation software, was used to complete the FE analysis in this thesis. Establishment of a FE model, the first step in each FE method, is implemented in this chapter.

2.1 Geometric model

To make FE study results accurate, geometric model must be realistic. To get realistic geometric model, a magnetic resonance (MR) image of human head was used in this study.

2.1.1 Magnetic resonance image

MRI is a medical imaging technique producing detailed images of organs, soft tissues, bone and virtually all other internal body structures to help physicians diagnose medical conditions [66]. MRI uses magnetic signals to create image “slices” of the human body, which are created based on differences among tissues. The anatomical structure of human

2.1 Geometric model

head is very complicated with many components in the head. To accurately evaluate various small abnormalities caused by diseases, high resolution imaging is necessary. Higher resolution image reflects more details. MR images have high resolution and they are able to non-invasively reveal the internal details of the human body. In comparison with other imaging techniques, such as X-ray, ultrasound imagining and CT, MRI offers higher image resolution and provides more detailed information of human body [66]. MRI also provides much greater contrast than CT and other medical imaging techniques. Contrast is the appearance difference of different tissues in an image. The high contrast of MR image makes the boundaries of all the internal body structures sharp enough for diagnosis and makes it especially useful in neurological imaging [66].

A MR image of a male adult's head is shown in Figure 2.1(a). Different intracranial components are shown in different colors. This image were taken at a position in the upper half of the human head, therefore, not all intracranial components can be seen from this image. The MR image contains geometry information of the displayed components. By using a software, e.g., MATLAB, the geometric model of the interested intracranial components can be obtained. In this study, the geometry of three main intracranial components, which are skull, cerebrospinal fluid and brain, were constructed from the MR image. Constructing and using the three main components geometry is more cost effective for FE study than getting the geometry of all the intracranial components since finding the correlation trend, or the correlation if it is possible, between ICP and external vibration responses is our first study goal. The geometry of the three main intracranial components constructed from the MR image was obtained by using MATLAB software,

2.1 Geometric model

and the geometry construction mainly involved "contour" functions in MATLAB. The main clue is described as follows.

First, read in the MR image to MATLAB by using "imread(filename)" function.

Second, using "contour(...,LineSpec)" function to draw the contours specified by line type and color which are in the MR image.

Third, specifying the contour levels with function "contour(*z*, *n*)". *z* is the data matrix, *n* is the number of contour lines.

Fourth, filling the contours with function "contour" which displays a 2D contour plot and fills the areas between contour lines with the specified colors.

The geometric model, which contains geometry information about skull, CSF and brain, used in this thesis is shown in Fig.2.1 (b).

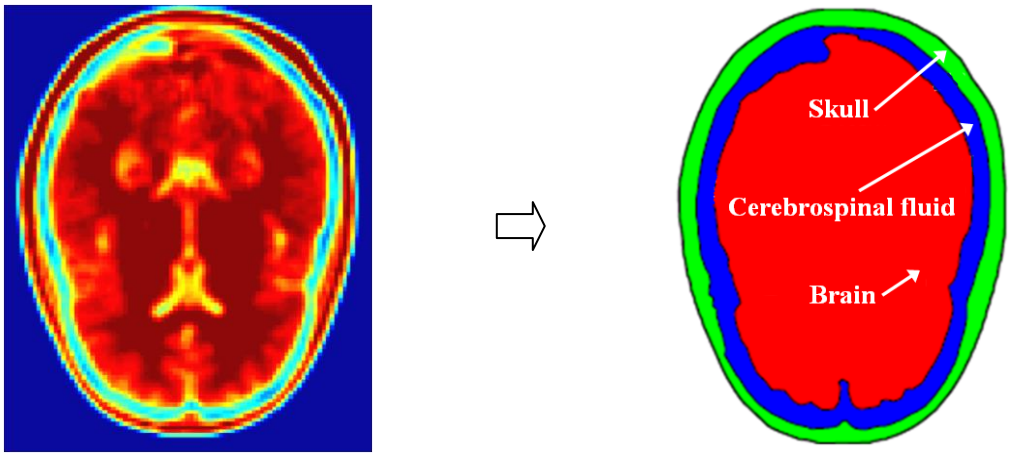

(a) MR image (b) Geometric model

Figure 2.1: Constructing a geometric model from a MR image

2.1.2 Plane strain model

2D human head FE model is more cost effective than a 3D human head FE model for studying effects of different boundary conditions, loading conditions and model parameters, e.g., material properties [64, 67]. Although the human head is much more complicated than a 2D model and it is possible to construct a 3D model for the head with advanced imaging technologies, a 2D model is adequate for the preliminary research conducted in this thesis. A 2D biomechanical model to solve problems in elasticity whose solutions (i.e., displacements and stresses) are not dependent on one of the coordinates because of their geometry, boundary conditions, and external applied loads, can be either built as a plane strain model or a plane stress model [65]. During 1980's and early 1990's, plane strain models were widely adopted in the study of dynamics of human head under various impacts, see [64] and the references therein. The case for normally using plane stress model is that when one dimension is very small compared to the other two dimensions. If one dimension is very large compared to the others, the principle strain in the direction of the longest dimension is constrained and can be assumed as zero, yielding a plane strain [65, 68]. Figure 2.2 shows a horizontal cross-section image of the human head. The image was constructed from the MR image, which was taken at location O-O' of the head. From Fig.2.2, it is easy to see that the length of the head in *z* direction is large in comparison with that in *x* and *y* direction. Therefore, a plane strain model is used here. The ICP applied in human head is indicated by expression $p(x, y)$ and it is applied in the *xy* plane in the plane strain model [68].

A plane strain model is characterized by [65]:

2.1 Geometric model

$$u_x = u_x(x, y), \quad u_y = u_y(x, y), \quad u_z = 0 \tag{2.1}$$

Where u_x , u_y, and u_z denote the displacements in *x*, *y* and *z* direction respectively, in a rectangular coordinate system. The strain components in the plane strain model have the following expressions [65]:

$$\varepsilon_z = \gamma_{xz} = \gamma_{yz} = 0$$

$$\varepsilon_x = \frac{\partial u_x}{\partial x}, \quad \gamma_{xy} = \frac{\partial u_x}{\partial y} + \frac{\partial u_y}{\partial x}, \quad \varepsilon_y = \frac{\partial u_y}{\partial y} \tag{2.2}$$

Where ε_x , ε_y , ε_z are the normal strains; and γ_{xz} , γ_{yz} , γ_{xy} are the shear strains.

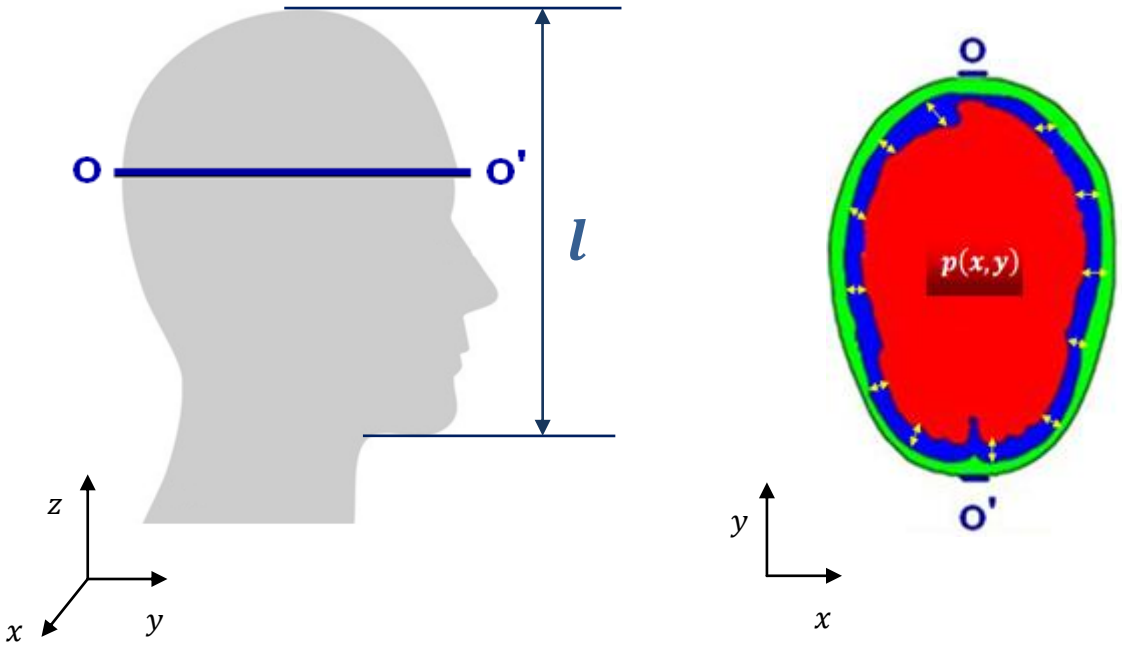

Figure 2.2: The geometric model constructed from a MR image, which was taken at a horizontal cross-section position of the human head

2.2 Material properties

Material properties influence a substance's response or behaviour under an external loading. The material properties of the components in human head are different. To build a 2D human head FE model, which is based on the geometric model (see section 2.1.1), the material properties of the three considered components (i.e., the skull, the CSF and the brain) are required, and they were obtained from literatures and listed in Table 2.1 [15, 16, 17].

Table 2.1: Material properties of the skull, brain and CSF in the human head

	Young's Modulus (MPa)	Bulk Modulus (MPa)	Poisson's Ratio	Mass Density (Kg/m^3)
Skull	6650.0	-	0.220	2080
Brain	0.5581	2190	0.485	1040
CSF	0.1485	2190	0.499	1040

Young's modulus is a measure of the stiffness of a given material. Table 2.1 shows that the Young's modulus of the skull which is much higher than that of the brain and the CSF. In other words, skull is much stiffer than brain and CSF. Bulk modulus measures a substance's resistance to uniform compression. In Table 2.1, the brain tissue and the CSF have the same bulk modulus, which is 2.19 GPa, and it is similar to that of water with the value of 2.1 GPa [17]. However, the skull bulk modulus has not been found from the reviewed literatures. Since it is not involved in the afterwards FE modeling, it is left blank

here. Poisson's ratio (ν) is a measure of the transverse deformation when a sample of material is stretched in one direction, and the material tends to get thinner in the other two directions perpendicular to the stretched direction. For a perfectly incompressible material, the Poisson's ratio would be exactly 0.5. As shown in Table 2.1, the CSF is nearly incompressible as indicated by its Poisson's ratio value of 0.499 which is very close to 0.5, while brain tissue is a slightly incompressible material and skull is a compressible material.

The material properties listed above were obtained from adults [15, 16, 17]. However, the tested objects' age, or age range were not given in the literatures.

2.3 Governing equations

Governing equations for a system, namely, are the equations that govern or determine a system's motion. Substance in different state, such as solid and fluid, are governed by different equations. In the studied 2D human head model, the skull and the brain were treated as solid and the CSF was considered as a fluid since only the particles in CSF can flow easily. The CSF interacts with the skull and the brain, neither the fluid part (CSF) nor the solid parts (the skull and the brain) can be solved independently due to the unknown interface forces. The fluid-solid interaction is a coupled problem, and the coupling occurs on domain interfaces via the boundary conditions imposed there [69]. For the skull and brain, and the CSF, the governing equations determine their behaviours are discussed in the following parts.

2.3 Governing equations

2.3.1 Skull and brain

Since skull and brain are considered as solid materials, if body forces are not considered, deriving from Newton's second law, their governing equation can be expressed as follows [70, 69]:

$$\boldsymbol{\nabla} \cdot \boldsymbol{\sigma} + \boldsymbol{\mu}\dot{\mathbf{u}} = \rho\ddot{\mathbf{u}} \tag{2.3}$$

Where ∇ is the differentiation operator; $\boldsymbol{\sigma}$ is the vector containing the relevant stress components; $\boldsymbol{\mu}$ is the matrix containing the damping coefficients of the solid materials; **u** denotes the displacement vector (a dot over **u** represents its derivative with respect to time); and ρ is the mass density of the material.

The expressions of vectors and matrices in Equation (2.1) are given as follows:

$$\boldsymbol{\nabla} = \begin{bmatrix} \frac{\partial}{\partial x} & 0 & \frac{\partial}{\partial y} \\ 0 & \frac{\partial}{\partial y} & \frac{\partial}{\partial x} \end{bmatrix}, \qquad \boldsymbol{\sigma} = \begin{Bmatrix} \sigma_x \\ \sigma_y \\ \tau_{xy} \end{Bmatrix}, \qquad \boldsymbol{\mu} = \begin{bmatrix} \mu_x & 0 \\ 0 & \mu_y \end{bmatrix}, \qquad \mathbf{u} = \begin{Bmatrix} u \\ v \end{Bmatrix} \tag{2.4}$$

The expanded form of the governing equations is

$$\frac{\partial \sigma_x}{\partial x} + \frac{\partial \tau_{xy}}{\partial y} + \mu_x \frac{\partial u}{\partial t} = \rho \frac{\partial^2 u}{\partial t^2} \tag{2.5}$$

$$\frac{\partial \sigma_y}{\partial y} + \frac{\partial \tau_{xy}}{\partial x} + \mu_y \frac{\partial v}{\partial t} = \rho \frac{\partial^2 v}{\partial t^2} \tag{2.6}$$

2.3.2 Cerebrospinal fluid

To establish the governing equations for the CSF, several assumptions have been made here. The assumptions are [69, 71, 72, 73]:

2.3 Governing equations

a) The density of CSF can be considered as a constant as its density varies only a small amount relative to its hydrostatic density. The CSF is a slightly compressible fluid (since its Poisson's ratio is 0.499).

b) The convective effects can be omitted in the CSF as the relative motion between the CSF and the solid parts is small and slow.

c) Stresses introduced by viscous effects can be neglected as CSF is considered as an inviscid fluid (its viscosity is 0.723×10^{-3} Pa·s which is the same as water).

The governing equation, which is a wave equation, for the CSF is [69, 70]:

$$\nabla^2 p = \frac{1}{c^2}\frac{\partial^2 p}{\partial t^2} \tag{2.7}$$

Where p is the acoustic pressure. c is the sound speed in the CSF and its expression is

$$c = \sqrt{\frac{K}{\rho_0}} \tag{2.8}$$

In the above expression, ρ_0 is the hydrostatic density of CSF; and K is the bulk modulus of CSF.

2.3.3 Boundary conditions

The boundary conditions for the human head model mainly considering the force equilibrium between the solid parts (skull and brain) and the fluid part (CSF). That is, the pressure from the fluid part equals to the inertia forces from the solid parts. The solid-fluid interaction can be described by [69],

$$\frac{\partial p}{\partial n} = -\rho_0 \dot{\bar{v}}_n = -\mathbf{n}^{\mathrm{T}} \cdot (\rho_0 \ \dot{\mathbf{v}}) \tag{2.9}$$

Where **v** is the fluid velocity, **n** is the interface outward normal pointing to the fluid region; $\bar{v}_n$ is the normal velocity; and p is the pressure. The velocity and the acceleration are obtained from displacement via:

$$\dot{\bar{v}}_n = \ddot{u}_n = \mathbf{n}^{\mathrm{T}} \ddot{\mathbf{u}} \tag{2.10}$$

Combining Equations (2.9) and (2.10), we can thus obtain the following equation as the boundary conditions:

$$\mathbf{n}^{\mathrm{T}} \nabla p = -\rho_0 \dot{\bar{v}}_n = -\mathbf{n}^{\mathrm{T}} \cdot (\rho_0 \ddot{\mathbf{u}}) \tag{2.11}$$

2.4 Finite element equations

Since analytical solutions are possible only for simple partial differential equations, approximate solutions are much easier to get by using a numerical method, e.g., FE method. That is, transform the partial differential equations of a continuum (the human head model here) to a set of algebraic equations of a discrete model (i.e., finite element) of the continuum. There are two steps for converting partial differential equations into algebraic equations. First, the partial differential equations are transformed into an equivalent variational formulation or integral formulation. Second, algebraic equations (FE equations) are obtained by introducing shape functions into the variational formulation and conducting variational operations. In the FE equations, shape function, matrices of mass, damping and stiffness are involved, and they are introduced in section 2.4.1 and section

2.4.2, respectively. This is followed by describing the Newmark method which is used to solve the FE equations.

2.4.1 Shape functions of quadrilateral element

Shape functions, also known as interpolation functions or blending functions, are used to express the unknown continuous field function by a set of known piecewise continuous functions and discrete unknown variables at element nodes [68]. For a univariate unknown continuous field function, it can be approximated as

$$\emptyset(x) \approx \sum_{i=1}^{n} N_i\,(x)\emptyset_{\mathrm{i}} \tag{2.12}$$

In Equation (2.12), N_i $(i = 1,2,\dots,n)$ are the shape functions; $\emptyset_{\mathrm{i}}$ are discrete function values at element nodes. The element types in ANSYS chosen for 2D modeling of solid structures (skull and brain) and fluid (CSF) are PLANE42 and FLUID29, which both have four nodes, and the desired element shape for them is four-node quadrilateral. The field variable for a four-node quadrilateral element in terms of natural coordinates, $-1 \le \xi \le 1$ and $-1 \le \eta \le 1$, can be expressed as

$$\emptyset(\xi,\eta) \approx \sum_{i=1}^{4} N_i\,(\xi,\eta)\emptyset_{\mathrm{i}} \tag{2.13}$$

In expression (2.13), i = 1, 2, 3, 4. The coordinates are $(\xi_1 = -1, \eta_1 = -1)$, $(\xi_2 = 1, \eta_2 = -1)$, $(\xi_3 = 1, \eta_3 = 1)$ and $(\xi_4 = -1, \eta_4 = 1)$ for the four nodes, respectively. The natural coordinates system is shown in Fig.2.3.

2.4 Finite element equations

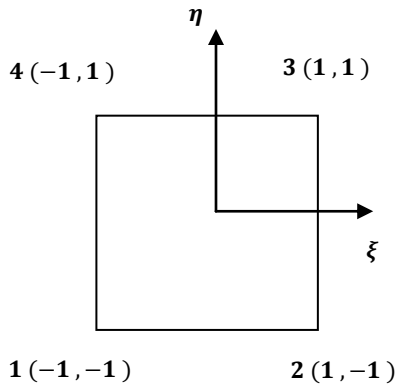

Figure 2.3: Natural coordinate system

The four-node quadrilateral element shape functions are defined in the natural coordinate system as

$$N_1(\xi,\eta) = \frac{1}{4}(1-\xi)(1-\eta)$$

$$N_2(\xi,\eta) = \frac{1}{4}(1+\xi)(1-\eta) \qquad (2.14)$$

$$N_3(\xi,\eta) = \frac{1}{4}(1+\xi)(1+\eta)$$

$$N_4(\xi,\eta) = \frac{1}{4}(1-\xi)(1+\eta)$$

The shape functions satisfy the so-called Kronecker-Delta conditions, i.e.,

$$(\xi,\eta) = (-1,-1) \Rightarrow (N_1 = 1, N_2 = 0, N_3 = 0, N_4 = 0)$$

$$(\xi,\eta) = (1,-1) \Rightarrow (N_1 = 0, N_2 = 1, N_3 = 0, N_4 = 0) \qquad (2.15)$$

$$(\xi,\eta) = (1,1) \Rightarrow (N_1 = 0, N_2 = 0, N_3 = 1, N_4 = 0)$$

$$(\xi,\eta) = (-1,1) \Rightarrow (N_1 = 0, N_2 = 0, N_3 = 0, N_4 = 1)$$

2.4 Finite element equations

Since the geometric model (see section 2.1) involves curved boudaries, and straightsided elements (e.g., square shape element) may not provide satisfactory results [74], isoparametric elements are required here. Isoparametric elements refer to the shape (or geometry) and the field variable of the elements are described by the same shape functions [74]. Therefore, the geometry representation in terms of shape functions can be regared as as a mapping procedure that transforms a regular quadrilateral in global coordinates to a square in local coordinates [74]. Figure 2.4 shows the quadrilateral element mapped from its global coordinate system to its natural coordinate system.

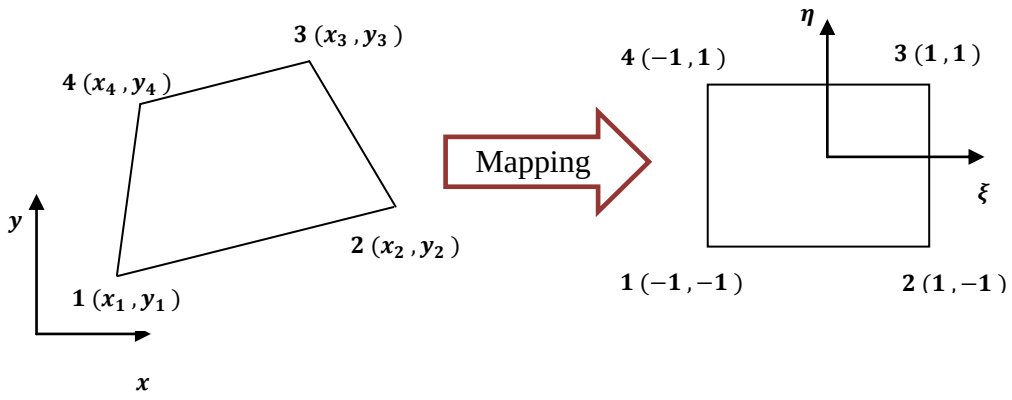

Figure 2.4: Quadrilateral element mapped from its global coordinate system to its natural coordinate system

So an arbitrary quadrilateral in global coordinates (x, y) can be mapped into a square shape defined in natural coordinates (ξ, η), achieved by

$$\begin{cases} x = N_1(\xi,\eta)x_1 + N_2(\xi,\eta)x_2 + N_3(\xi,\eta)x_3 + N_4(\xi,\eta)x_4 \\ y = N_1(\xi,\eta)y_1 + N_2(\xi,\eta)y_2 + N_3(\xi,\eta)y_3 + N_4(\xi,\eta)y_4 \end{cases} \tag{2.16}$$

2.4 Finite element equations

Hence, the field variable can be expressed as

$$\emptyset(x,y) = \emptyset(\xi,\eta) = N_1(\xi,\eta)\emptyset_1 + N_2(\xi,\eta)\emptyset_2 + N_3(\xi,\eta)\emptyset_3 + N_4(\xi,\eta)\emptyset_4 \tag{2.17}$$

The variables x and y are changed to ξ and η since the integrals can be evaluated using natural coordinates which has more advantages than global coordinate systems. Thus, the integral over an arbitrary quadrilateral region of $dxdy$ becomes a square area of $d\xi d\eta$ in a natural coordinate systems in the form of [74]:

$$\int_A \emptyset(x,y)dxdy = \int_{-1}^{1}\int_{-1}^{1} \emptyset(\xi,\eta)|\mathbf{J}|\, d\xi d\eta \tag{2.18}$$

Where $|\mathbf{J}|$ is the determinant of the Jacobian matrix which relates the term $dxdy$ and $d\xi d\eta$ as [74]

$$dxdy = |\mathbf{J}|d\xi d\eta \tag{2.19}$$

The Jacobian matrix, $\mathbf{J}$ is given by

$$[\,\mathbf{J}\,] = \begin{bmatrix} \dfrac{\partial x}{\partial \xi} & \dfrac{\partial y}{\partial \xi} \\ \dfrac{\partial x}{\partial \eta} & \dfrac{\partial y}{\partial \eta} \end{bmatrix} \tag{2.20}$$

The determinant of the Jacobian matrix is always positive, $|\mathbf{J}| > 0$, for a one-to-one mapping [74].

2.4.2 Mass, damping and stiffness matrices

Finite element equations of the solid parts, which converted from governing equation 2.3, are put in matrix form [70]:

$$\mathbf{M}^{\mathrm{s}}\ddot{\tilde{\mathbf{u}}} + \mathbf{C}^{\mathrm{s}}\dot{\tilde{\mathbf{u}}} + \mathbf{K}^{\mathrm{s}}\tilde{\mathbf{u}} - \mathbf{Q}\,\tilde{\mathbf{p}} = 0 \tag{2.21}$$

Where $\mathbf{M}^{\mathrm{s}}$, $\mathbf{C}^{\mathrm{s}}$, and $\mathbf{K}^{\mathrm{s}}$ are, respectively, the mass, damping and stiffness matrices of the skull and the brain. $\tilde{\mathbf{u}}$ represents the discrete value of displacement at an element node (a dot and two dots over a variable, for example, $\dot{\tilde{\mathbf{u}}}$ and $\ddot{\tilde{\mathbf{u}}}$, represent its first and second derivate over time, respectively). $\mathbf{Q}$ is the fluid-solid coupling matrix. $\tilde{\mathbf{p}}$ stands for the discrete stress value at an element node from CSF. The expressions of the matrices are given as follows:

Mass matrix:

$$\mathbf{M}^{\mathrm{s}} = \int_{\Omega_{\mathrm{s}}} \rho_s \mathbf{N}_{\mathrm{u}}^T \mathbf{N}_{\mathrm{u}}\, d\Omega \tag{2.22}$$

Where ρ_s is the density of the solid parts. $\boldsymbol{N}_{\mathrm{u}}$ contains the shape functions of element displacements. Ω_{s} is the domain occupied by the solid part.

Damping matrix:

$$\mathbf{C}^{\mathrm{s}} = \int_{\Omega_{\mathrm{s}}} \mathbf{N}_{\mathrm{u}}^T \boldsymbol{\mu} \mathbf{N}_{\mathrm{u}}\, d\Omega \tag{2.23}$$

Where $\boldsymbol{\mu}$ contains damping coefficients of solid materials.

Stiffness matrix:

2.4 Finite element equations

$$\mathbf{K}^{\mathrm{s}} = \int_{\Omega_{\mathrm{s}}} \mathbf{B}_{\mathrm{s}}^{T} \mathbf{D} \mathbf{B}_{\mathrm{s}} \, d\Omega \tag{2.24}$$

Where $\mathbf{B}_{\mathrm{s}}$ is the strain-displacement matrix. $\mathbf{D}$ is the material property matrix.

Fluid- solid coupling matrix:

$$\mathbf{Q} = \int_{S} \mathbf{N}_{\mathrm{u}}^{T} \mathbf{n} \mathbf{N}_{\mathrm{p}} \, dS \tag{2.25}$$

Where $\mathbf{n}$ is the normal of a fluid-solid interface pointing to the fluid domain. $\mathbf{N}_{\mathrm{p}}$ contains the shape functions of element pressure. S represents the fluid-solid interface in the human head model.

Finite element equations of the fluid part, which obtained in reference to Equation (2.7), is [69]:

$$\mathbf{M}^{\mathrm{f}} \ddot{\tilde{\mathbf{p}}} + \mathbf{C}^{\mathrm{f}} \dot{\tilde{\mathbf{p}}} + \mathbf{K}^{\mathrm{f}} \tilde{\mathbf{p}} + \rho_0 \mathbf{Q}^{T} \ddot{\tilde{\mathbf{u}}} = \mathbf{0} \tag{2.26}$$

Where $\mathbf{M}^{\mathrm{f}}$, $\mathbf{C}^{\mathrm{f}}$, $\mathbf{K}^{\mathrm{f}}$ are, respectively, the mass, damping and stiffness matrices of the fluid part. ρ_0 is the hydrostatic density of the CSF. The expressions of the matrices in the above equation are given as follows [69]:

Mass matrix:

$$\mathbf{M}^{\mathrm{f}} = \int_{\Omega_{\mathrm{f}}} \mathbf{N}_{\mathrm{p}}^{T} \frac{\mathbf{1}}{c^2} \mathbf{N}_{\mathrm{p}} \, d\Omega \tag{2.27}$$

Where c is the sound speed in CSF; and Ω_{f} is the domain occupied by the fluid part.

Damping matrix:

2.4 Finite element equations

$$\mathbf{C}^{\mathrm{f}} = \int_S \mathbf{N}_{\mathrm{p}}^T \frac{\mathbf{1}}{c} \mathbf{N}_{\mathrm{p}}\, dS \tag{2.28}$$

Stiffness matrix:

$$\mathbf{K}^{\mathrm{f}} = \int_{\Omega_{\mathrm{f}}} (\boldsymbol{\nabla}\mathbf{N}_{\mathrm{p}})^T \boldsymbol{\nabla}\mathbf{N}_{\mathrm{p}} d\Omega \tag{2.29}$$

Combining FE equations of the solid part and the fluid part together, FE equations for the whole human head model can be expressed as [70]:

$$\begin{bmatrix} \mathbf{M}^{\mathrm{s}} & \mathbf{0} \\ \rho_0 \mathbf{Q}^T & \mathbf{M}^{\mathrm{f}} \end{bmatrix} \begin{Bmatrix} \ddot{\tilde{\mathbf{u}}} \\ \ddot{\tilde{\mathbf{p}}} \end{Bmatrix} + \begin{bmatrix} \mathbf{C}^{\mathrm{s}} & \mathbf{0} \\ \mathbf{0} & \mathbf{C}^{\mathrm{f}} \end{bmatrix} \begin{Bmatrix} \dot{\tilde{\mathbf{u}}} \\ \dot{\tilde{\mathbf{p}}} \end{Bmatrix} + \begin{bmatrix} \mathbf{K}^{\mathrm{s}} & \mathbf{0} \\ \mathbf{0} & \mathbf{K}^{\mathrm{f}} \end{bmatrix} \begin{Bmatrix} \tilde{\mathbf{u}} \\ \tilde{\mathbf{p}} \end{Bmatrix} = \begin{Bmatrix} \mathbf{0} \\ \mathbf{0} \end{Bmatrix} \tag{2.30}$$

To solve the above FE equations, the Newmark method was used and the following section discusses that in detail.

2.4.3 Newmark method

Newmark method is a family of single-step integration method for the solution of structural dynamic problems. By using one of the Newmark methods, the variables $\tilde{\mathbf{u}}$ and $\dot{\tilde{\mathbf{u}}}$ in FE equation (2.21) can be expressed as [75]

$$\tilde{\mathbf{u}}_t = \tilde{\mathbf{u}}_{t-\Delta t} + \Delta t \dot{\tilde{\mathbf{u}}}_{t-\Delta t} + \frac{\Delta t^2}{2} \ddot{\tilde{\mathbf{u}}}_{t-\Delta t} + \beta \Delta t^3 \dddot{\tilde{\mathbf{u}}}_{t-\Delta t} \tag{2.31}$$

$$\dot{\tilde{\mathbf{u}}}_t = \dot{\tilde{\mathbf{u}}}_{t-\Delta t} + \Delta t \ddot{\tilde{\mathbf{u}}}_{t-\Delta t} + \gamma \Delta t^2 \dddot{\tilde{\mathbf{u}}}_{t-\Delta t} \tag{2.32}$$

2.4 Finite element equations

The integration parameters in equations (2.31) and (2.32) are usually taken as $\beta = 1/4$ and $\gamma = 1/2$. If acceleration $\ddot{\mathbf{u}}$ is assumed to be linear within the time step, the third time derivative of displacement can be written as

$$\dddot{\mathbf{u}}_{t-\Delta t} = \frac{\ddot{\mathbf{u}}_t - \ddot{\mathbf{u}}_{t-\Delta t}}{\Delta t} \tag{2.33}$$

Substitute Equation (2.33) into Equations (2.31) and (2.32), the standard form of Newmark's equations can be expressed as

$$\tilde{\mathbf{u}}_t = \tilde{\mathbf{u}}_{t-\Delta t} + \Delta t\dot{\tilde{\mathbf{u}}}_{t-\Delta t} + (\frac{1}{2} - \beta)\Delta t^2\ddot{\tilde{\mathbf{u}}}_{t-\Delta t} + \beta\Delta t^2\ddot{\tilde{\mathbf{u}}}_t \tag{2.34}$$

$$\dot{\tilde{\mathbf{u}}}_t = \dot{\tilde{\mathbf{u}}}_{t-\Delta t} + (1-\gamma)\Delta t\ddot{\tilde{\mathbf{u}}}_{t-\Delta t} + \gamma\Delta t\ddot{\tilde{\mathbf{u}}}_t \tag{2.35}$$

Due to FE Equation (2.21) involves stiffness and mass proportional damping, Newmark's method in matrix notation which is formulated by Wilson [76] is introduced here. Equations (2.34) and (2.35) can be rewritten in the following form:

$$\ddot{\tilde{\mathbf{u}}}_t = b_1(\tilde{\mathbf{u}}_t - \tilde{\mathbf{u}}_{t-\Delta t}) + b_2\dot{\tilde{\mathbf{u}}}_{t-\Delta t} + b_3\ddot{\tilde{\mathbf{u}}}_{t-\Delta t} \tag{2.36}$$

$$\dot{\tilde{\mathbf{u}}}_t = b_4(\tilde{\mathbf{u}}_t - \tilde{\mathbf{u}}_{t-\Delta t}) + b_5\dot{\tilde{\mathbf{u}}}_{t-\Delta t} + b_6\ddot{\tilde{\mathbf{u}}}_{t-\Delta t} \tag{2.37}$$

Where

$$b_1 = \frac{1}{\beta\Delta t^2}, \quad b_2 = \frac{1}{\beta\Delta t}, \quad b_3 = 1 - \frac{1}{2\beta}, \quad b_4 = \frac{\gamma}{\beta\Delta t},$$
$$b_5 = 1 - \frac{\gamma}{\beta}, \quad b_6 = \Delta t\left(1 - \frac{\gamma}{2\beta}\right) \tag{2.38}$$

2.4 Finite element equations

At time t, substitute equations (2.36) and (2.37) into equation (2.21) which can be expressed as

$$(b_1\mathbf{M}^s + b_4\mathbf{C}^s + \mathbf{K}^s)\tilde{\mathbf{u}}_t = \mathbf{M}^s\left(b_1\tilde{\mathbf{u}}_{t-\Delta t} - b_2\dot{\tilde{\mathbf{u}}}_{t-\Delta t} - b_3\ddot{\tilde{\mathbf{u}}}_{t-\Delta t}\right)$$
$$+\mathbf{C}^s\left(b_4\tilde{\mathbf{u}}_{t-\Delta t} - b_5\dot{\tilde{\mathbf{u}}}_{t-\Delta t} - b_6\ddot{\tilde{\mathbf{u}}}_{t-\Delta t}\right) + \mathbf{Q}\,\tilde{\mathbf{p}} \qquad (2.39)$$

Define an effective stiffness matrix as

$$\overline{\mathbf{K}} = b_1\mathbf{M}^s + b_4\mathbf{C}^s + \mathbf{K}^s \qquad (2.40)$$

And the effective load vector is

$$\overline{\mathbf{F}_t} = \mathbf{M}^s\left(b_1\tilde{\mathbf{u}}_{t-\Delta t} - b_2\dot{\tilde{\mathbf{u}}}_{t-\Delta t} - b_3\ddot{\tilde{\mathbf{u}}}_{t-\Delta t}\right) +$$
$$\mathbf{C}^s\left(b_4\tilde{\mathbf{u}}_{t-\Delta t} - b_5\dot{\tilde{\mathbf{u}}}_{t-\Delta t} - b_6\ddot{\tilde{\mathbf{u}}}_{t-\Delta t}\right) + \mathbf{Q}\,\tilde{\mathbf{p}} \qquad (2.41)$$

Consequently, the FE Equation (2.21) can be written as

$$\left[\,\overline{\mathbf{K}}\,\right]\{\,\tilde{\mathbf{u}}_t\} = \{\,\overline{\mathbf{F}_t}\,\} \qquad (2.42)$$

Then specify initial conditions $\dot{\tilde{\mathbf{u}}}_0$, $\ddot{\tilde{\mathbf{u}}}_0$.

For each time step ($t = \Delta t,\ 2\Delta t,\ 3\Delta t \ldots\ldots$), the following steps are used to calculate nodal displacement.

A. Calculate effective load vector $\overline{\mathbf{F}_t}$ using Equation (2.41)

B. Solve for node displacement vector at time t

$$\overline{\mathbf{K}}\ \tilde{\mathbf{u}}_t\ =\ \overline{\mathbf{F}_t}$$

Calculate node accelerations and velocities at time t using equations (2.36) and (2.37).

C. Go to step A with $t = t + \Delta t$.

Above is the clue for solving the FE equations of the skull and brain by using the Newmark method. The procedure for solving the FE equations of CSF is the same. In the study, the FE equations were solved by using ANSYS software. In ANSYS, there is a solution interface (called the Solution Controls dialog box) for setting analysis options. Transient, one tab of the Solution Controls dialog box, contains a subsequent tab called time integration and the time integration method can be specified there. The Newmark algorithm was chosen, and the integration parameters β and γ were defined as 0.25 and 0.5, respectively.

2.5 Establishment of 2D FE model of human head in ANSYS

ANSYS software is widely used in the computer-aided engineering field for FE analysis. It allows a design evaluation without having to build multiple prototypes in testing since it can realize model construction, applying operating loads and studying physical responses. In this section, a 2D human head FE model was established by using ANSYS, which was realized in the pre-processing stage of a FE method. Pre-processing involves geometry modeling, element selection, material representation and element mesh. The operations of establishing the 2D human head FE model in ANSYS is illustrated as follows:

2.5 Establishment of 2D FE model of human head in ANSYS

1. Geometry modeling. The geometric model of human head was constructed in MATLAB (see section 2.1) and imported to ANSYS. The imported 2D geometric model in ANSYS is shown in Figure 2.5.

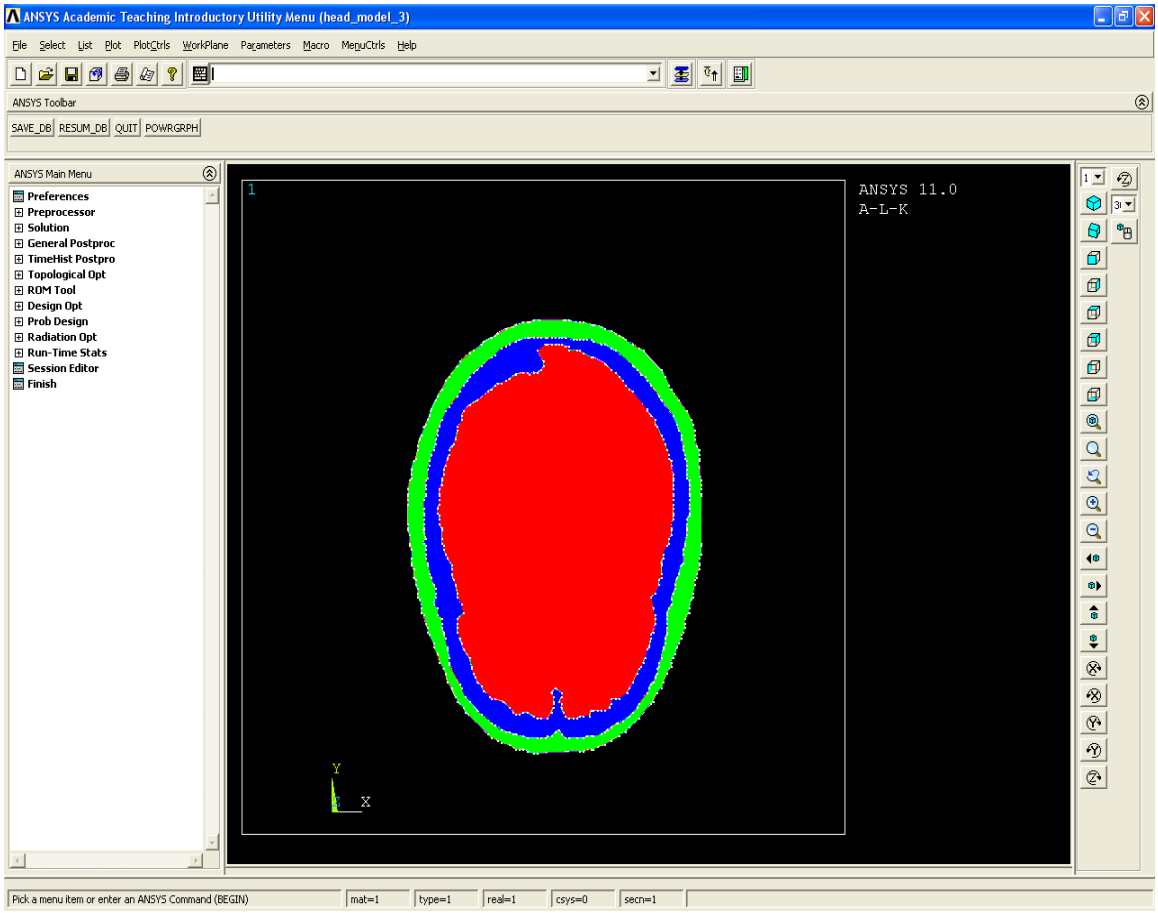

Figure 2.5: 2D geometric model of human head in ANSYS

2. Element selection. Element type determines the degree-of-freedom set (which in turn implies the discipline - structural, thermal, magnetic, electric, quadrilateral, brick, etc.) and whether the element lies in 2D or 3D space [77]. PLANE42 is chosen for the skull and brain, while FLUID29 is chosen for the CSF. PLANE42 is used for 2D modeling of

solid structures. The element has four nodes and with two degrees of freedom per node: translations in the nodal *x* and *y* directions [77]. It has plasticity, creep, swelling, stress stiffening, large deflection, large strain capabilities, etc. [77]. FLUID29 is used for modeling the fluid medium and interface in fluid/structure interaction problems [77]. Sound wave propagation and submerged structure dynamics are its two typical applications [77]. FLUID29 is defined by four nodes having three degrees of freedom per node: translations in the nodal x and y directions and pressure. The element can be used with other 2D structural elements to perform unsymmetric or damped modal, full transient analyses, and it has the capability to include damping of sound absorbing material at the interface [77].

Define the element types, point to the appropriate type reference number using the **TYPE** command or through the Graphic User Interface (**Main Menu > Preprocessor > Element Type > Add/Edit/Delete > Add… > Library of Element Types**, choose the element type and type the element reference number there. Then define element behaviors in the appeared **Element Type** tab, use the following: **Element Type > Options… > Element Behavior**, choose "plane strain" for PLANE42, and "Planar" for FLUID29.

3. Material representation. For each type of element, it may have multiple element property sets, ANSYS identifies each set with a unique reference number. The Material Model Number 1 (represent the skull material) was defined as: linear, isotropic, Young's modulus = 6650 MPa, Poisson's ratio = 0.22, and density = 2080 Kg/m^3. Material Model Number 2 (represent the brain material) was defined as: linear, isotropic, Young's modulus = 0.5581 MPa, Poisson's ratio = 0.485, and density = 1040 Kg/m^3. Material Model Number 3(represent the CSF material) was defined as: acoustics, density = 1040

Kg/m^3, sonic velocity = $\sqrt{\frac{k}{\rho}}$ = 1451.13 m/s (where k is the bulk modulus of the CSF and ρ is the density of the CSF), boundary admittance = 0.2. Boundary admittance is the quotient of the relative particle velocity and the sound pressure at the boundary. Figure 2.6 shows the interface of defining human head materials in ANSYS.

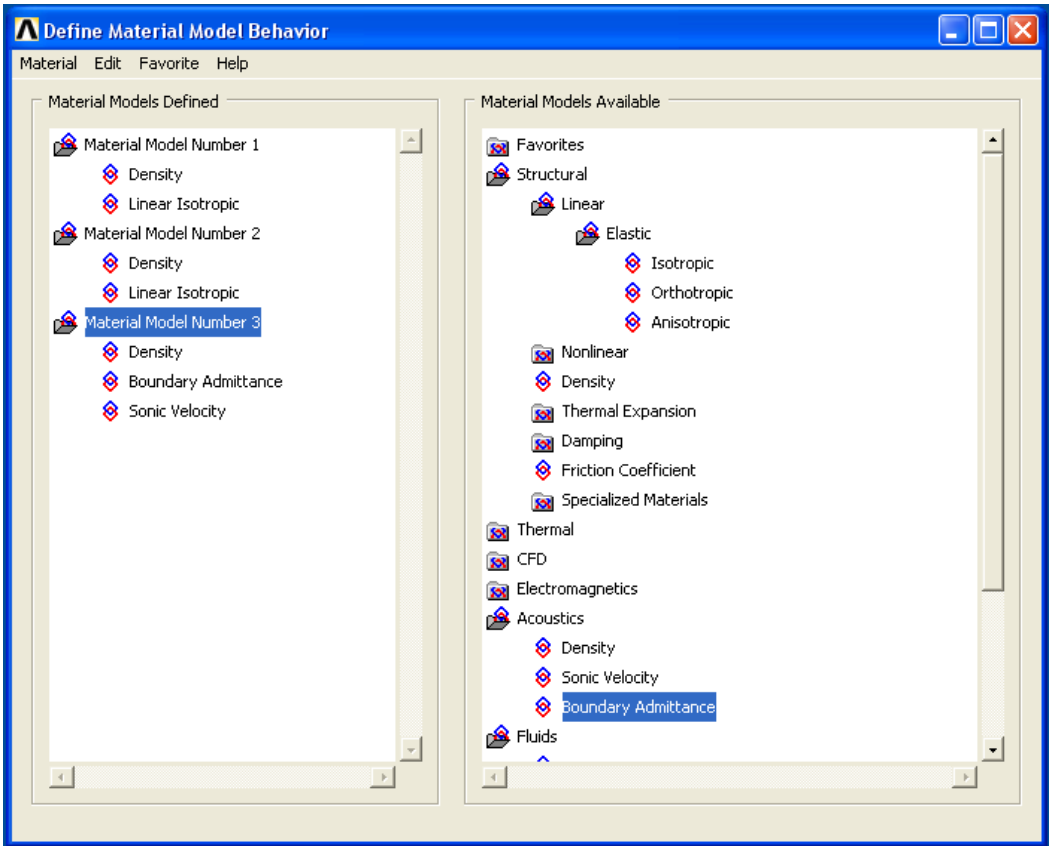

Figure 2.6: Interface of defining human head materials in ANSYS

The material properties were defined in the Graphic User Interface by following the steps: **Main Menu > Preprocessor > Material Props > Material Models > Define Material Model Behavior**, then input the material properties to the corresponding material model.

2.5 Establishment of 2D FE model of human head in ANSYS

4. Element mesh. Figure 2.7 displays the meshed 2D human head FE model. The element shape of all the three areas (the skull, brain and CSF) is quadrilateral. And the element size which affects the accuracy and economy of the analysis was 6 (The default value is 6, and the range of the size is from 1 to 10). The meshing type used is free mesh. There are 4967 elements and 5111 nodes in the FE model of human head. All the above mesh controls were realized in the ANSYS MeshTool (**Main Menu> Preprocessor> Meshing> MeshTool**).

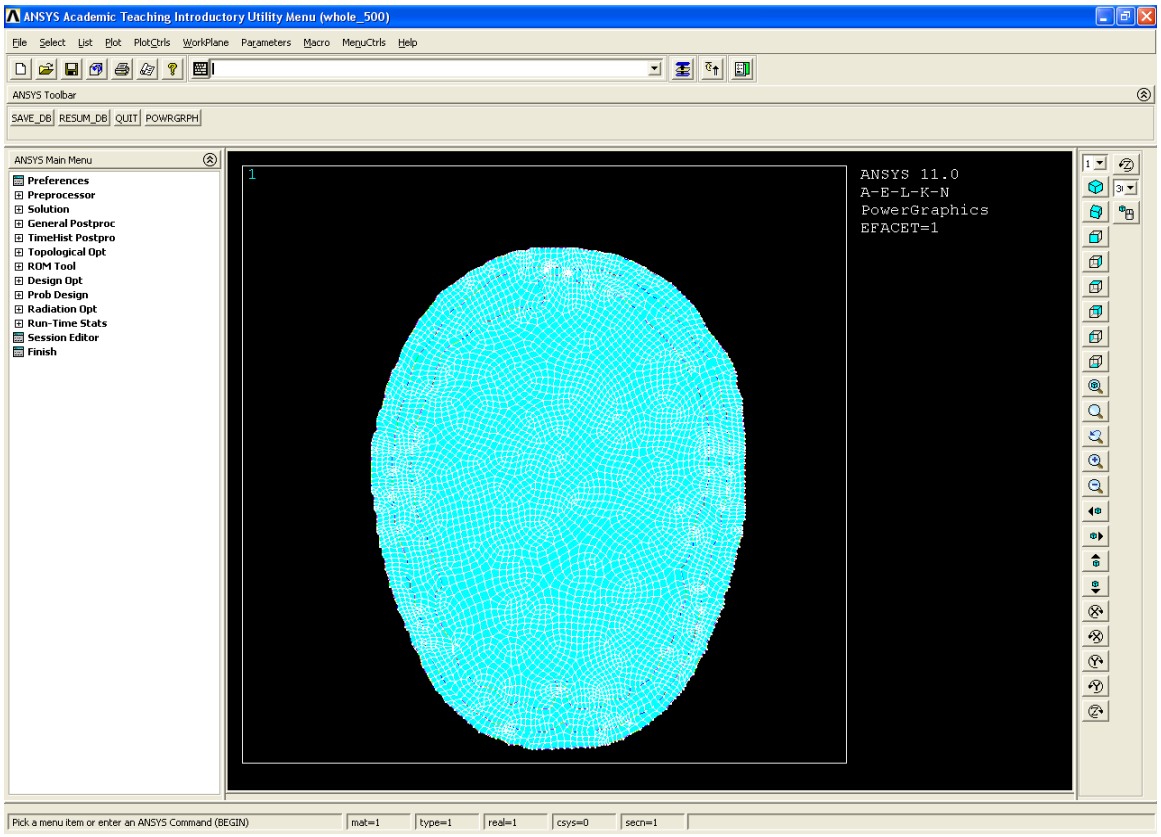

Figure 2.7: 2D FE model of human head in ANSYS

Chapter 3

Finite Element Study of Correlations between ICP and External Vibration Responses of Human Head

In this chapter, correlations between ICP and four vibration responses, which are displacement, velocity, acceleration and equivalent strain, are investigated in Section 3.1. To find out a good correlation for determining ICP, the magnitude and duration of applied impact, which may have effects on the correlations, are studied and discussed in Section 3.2 and Section 3.3, respectively.

3.1 Correlations establishment

Correlations between ICP and the four external vibration responses (i.e., displacement, velocity, acceleration and equivalent strain) of human head were explored in solution

stage and post-processing stage of a FE method. Solution stage includes specifying boundary and loading conditions, executing computation sequence and extracting numerical results. Post-processing involves the presentation and interpretation of the computed results [78].

In one solution stage, a particular ICP was applied to the 2D FE model of human head which was established in the pre-processing stage (see chapter 2). According to experimental data reported in [12, 20, 22, 23, 24], the normal range of ICP is approximately from 3.75 ~15 mm Hg, or between 500 ~ 2000 Pa. ICP higher than 15 mmHg or larger than 2000 Pa is considered as abnormal. Eleven ICP values were uniformly selected from the above two ranges. They are 500 Pa, 1000 Pa, 1500 Pa, 2000 Pa, 2500 Pa, 3000 Pa, 3500 Pa, 4000 Pa, 4500 Pa, 5000 Pa and 5500 Pa. An impact, in the form of step impulse, was applied to the human head model. In practice, the applied impact should harmless to human head and also generates strong enough vibration for getting good correlation between ICP and external vibration responses. In Willinger et al.'s study, they assume the intracerebral tissues can resist a compression of 200 kPa and a tension of 270 kPa during a 6 ms duration impact which were caused by a 6 kg impactor at 6.3 m/s, and the values were lower than those proposed as brain tolerance thresholds by Ward et al (compression: 234 kPa, tension: 2186 kPa) [79, 80]. In this study, we assume a 5 N force (i.e., a 0.51 kg impactor) with a duration of 10 ms is harmless to human head. Smaller impact that can generate strong vibration is also possible. The applied ICP and the step impulse are the loading conditions. ICP was applied at the interfaces between the skull and the CSF, the CSF and the brain, while the step impulse was applied at location A of the human head model. The boundary conditions were applied at location C and D. Displacement value at

location C and D were set as 0. All degrees of freedom of location D are constrained, while the degree-of-freedom of location C at *x* direction is constrained. Applying a boundary condition at location C is because if there is no constraint applied at location C (or some nearby place), any movement of the head will influence the measured responses. When a patient lying on bed, location D which is at the back part of the head is fixed, so constraint at location D is required. Having the constraint at location D is to make the studied results more applicable in practice. Each loading in the solution stage were saved as a LS (Loading step) file. Then conduct the FE analysis, which is transient analysis used in the thesis, and solve the problem from the saved LS files. Figure 3.1 shows an impact in the form of step impulse applying on the human head.

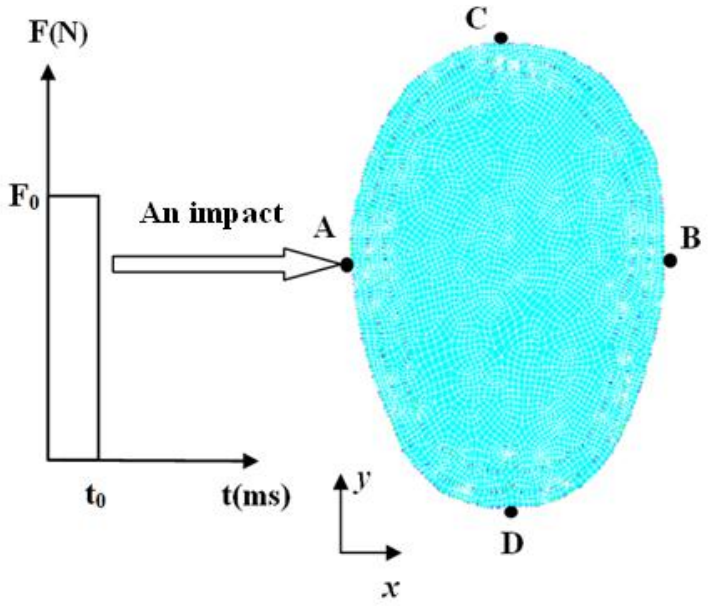

Figure 3.1: An impact in the form of step impulse applying on human head

3.1 Correlations establishment

The vibration responses (i.e., displacement, velocity, acceleration and equivalent strain) at location B were collected, the collecting time was 100 ms. Selection of position B for picking up responses is based on the consideration of the convenience on installing the transducer. Eleven sets of solution and post-processing were carried out. The applied ICP was the only difference among the sets. Time histories of the collected vibration responses are shown in Figure 3.2.

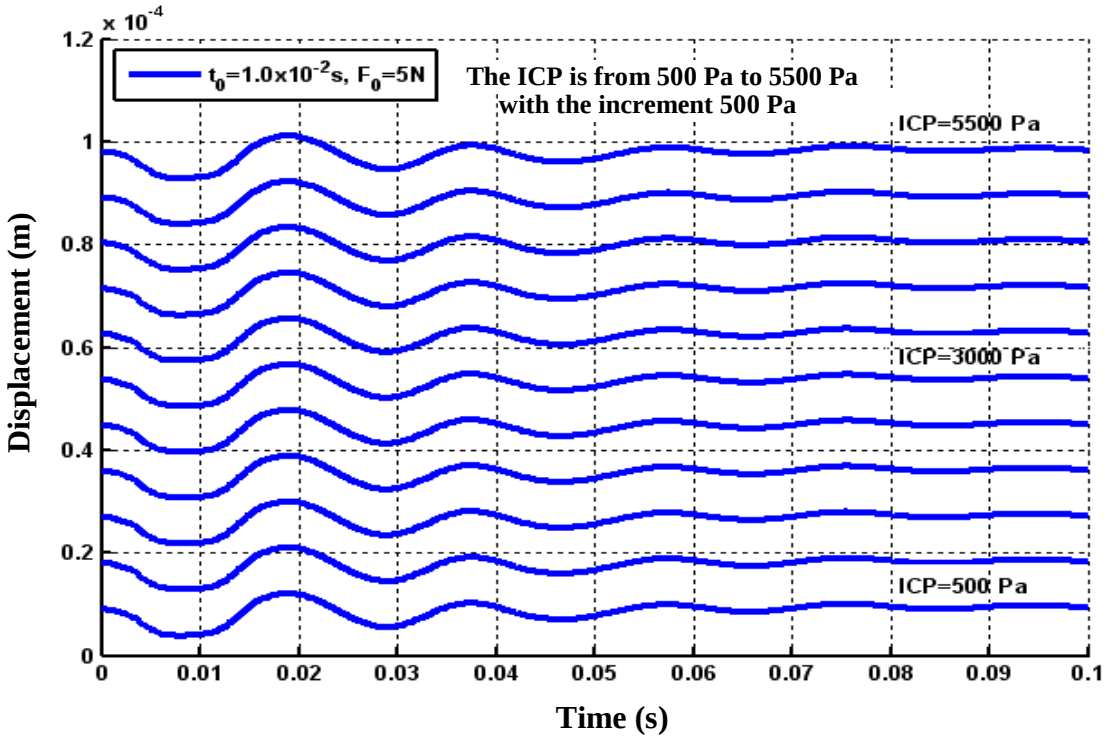

Figure 3.2 (a): Time histories of *x* direction displacement

3.1 Correlations establishment

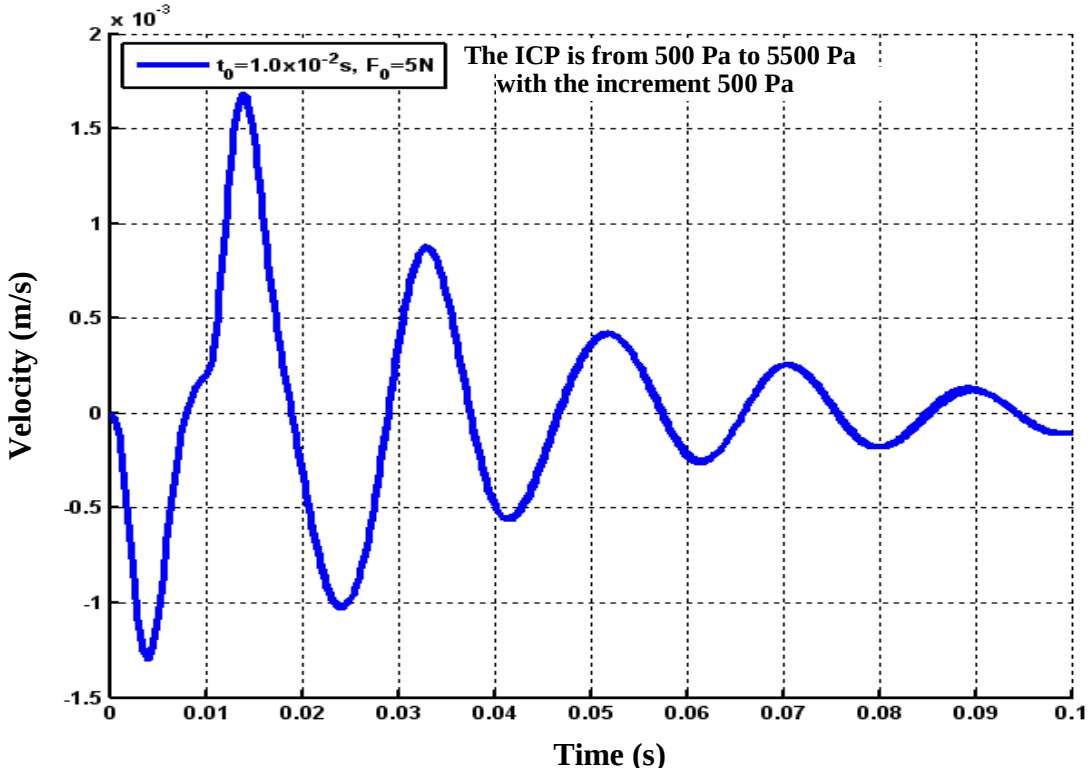

Figure 3.2 (b): Time histories of *x* direction velocity

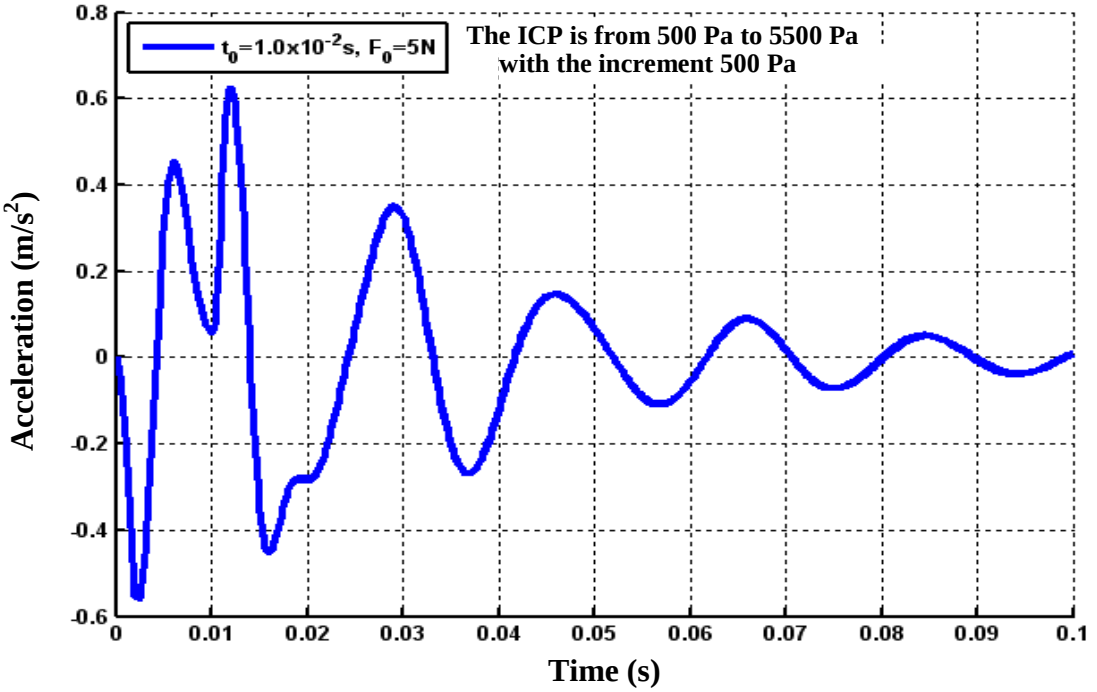

Figure 3.2 (c): Time histories of *x* direction acceleration

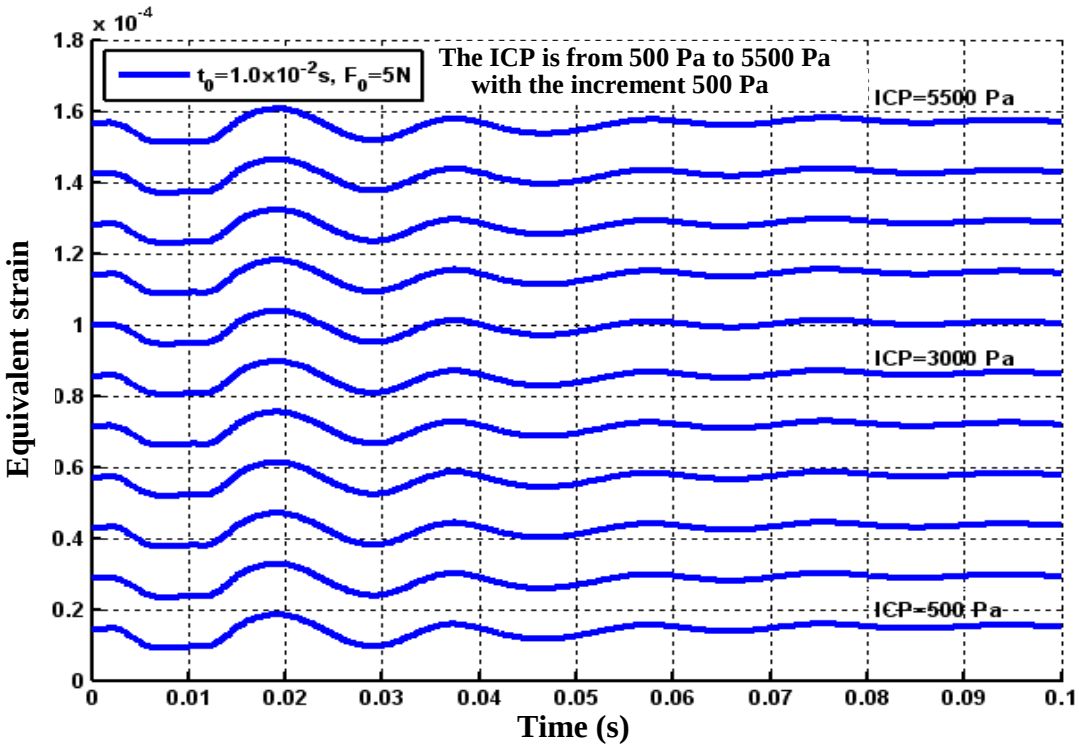

Figure 3.2 (d): Time histories of equivalent strain

It can be seen from Fig.3.2 that the time histories of the displacement and the equivalent strain are different for different ICP. However, both the velocity and the acceleration time histories changed little with ICP. In other words, displacement and equivalent are more sensitive to ICP change than velocity and acceleration. The difference of ICP effects on the responses may due to the initial stress fields introduced by ICP. ICP produces initial stress fields in the head, which is in the form of displacement and equivalent strain, and different ICP produces different displacement and different equivalent strain. However, ICP does not produce velocity or acceleration.

There are two reasons for collecting *x* direction responses. First, *x* direction responses are more dominant than *y* direction responses under the impact applied in *x* direction.

3.1 Correlations establishment

Second, they can be more easily picked up by a sensor installed at location B. To find a specific correlation between ICP and external vibration responses, peak values of the collected responses, displacement (u_x^{max}), velocity (v_x^{max}), acceleration (a_x^{max}) and equivalent strain (ε_e^{max}), were extracted from the data list file of the collected responses by using MATLAB. Correlation curves of ICP and the four investigated vibration responses are shown in Figure 3.3.

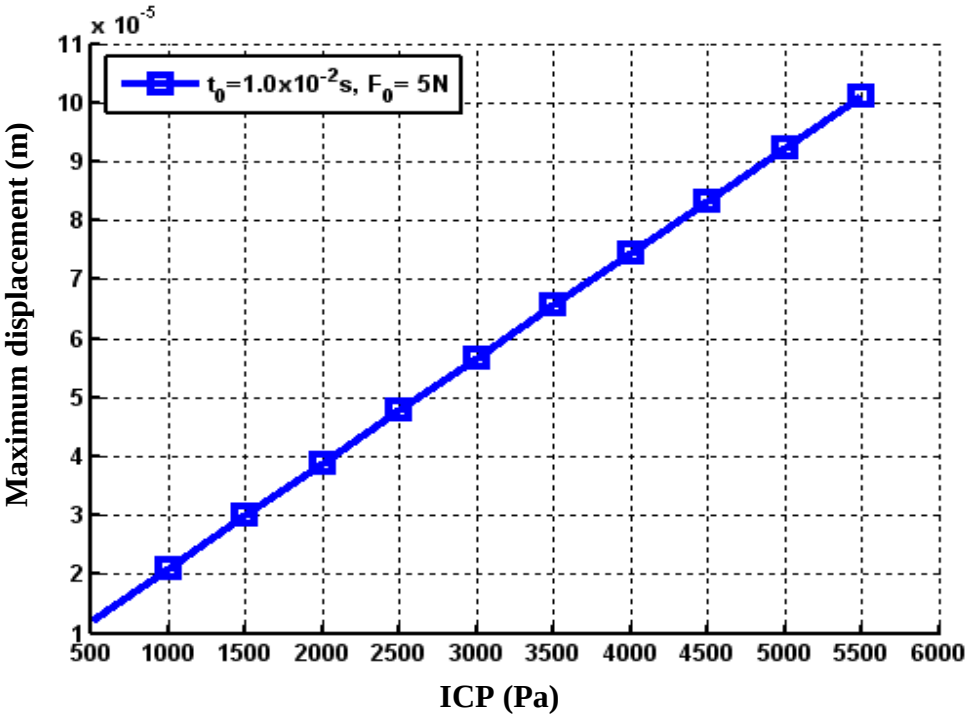

Figure 3.3 (a): Correlation between ICP and u_x^{max}

3.1 Correlations establishment

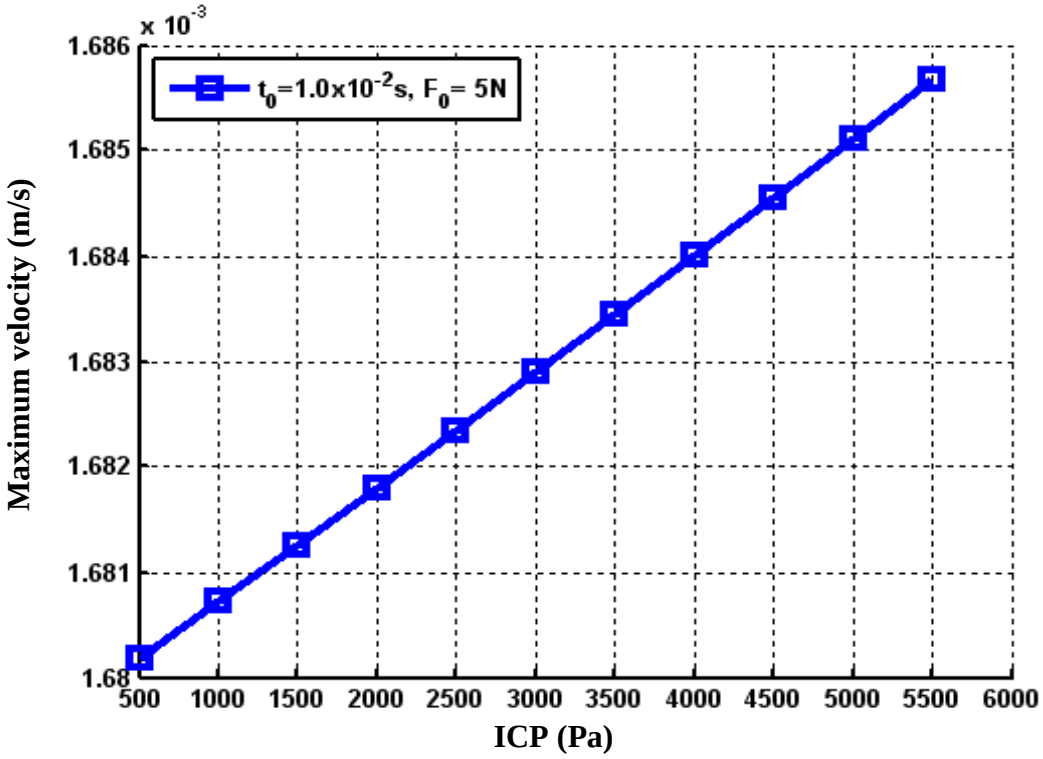

Figure 3.3 (b): Correlation between ICP and v_x^{max}

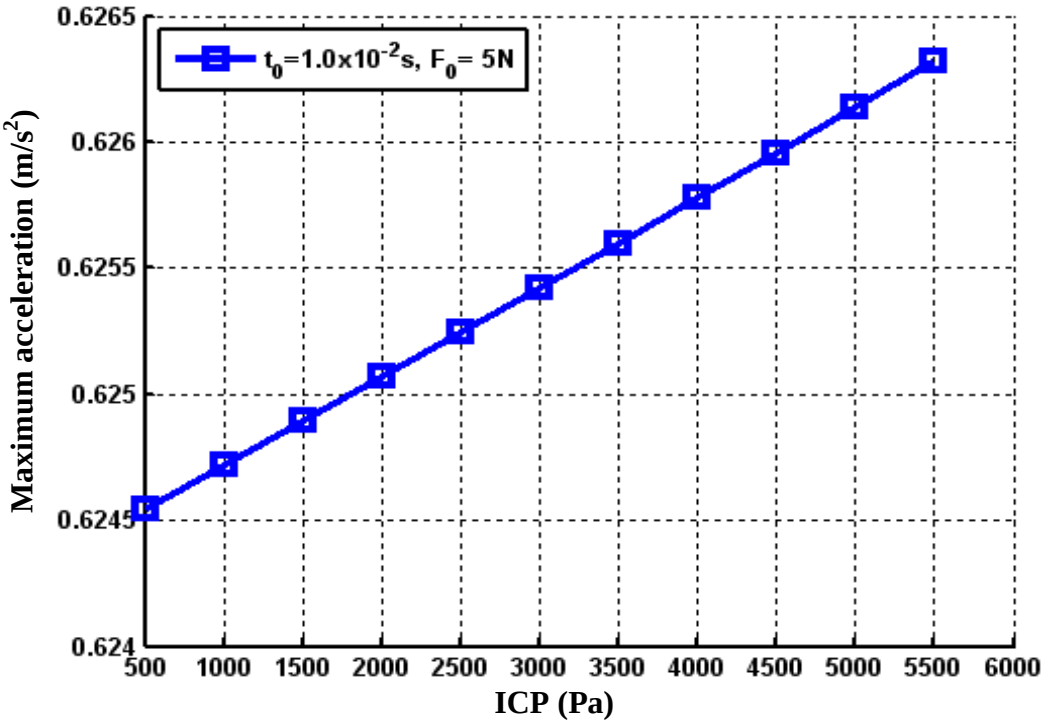

Figure 3.3 (c): Correlation between ICP and a_x^{max}

3.1 Correlations establishment

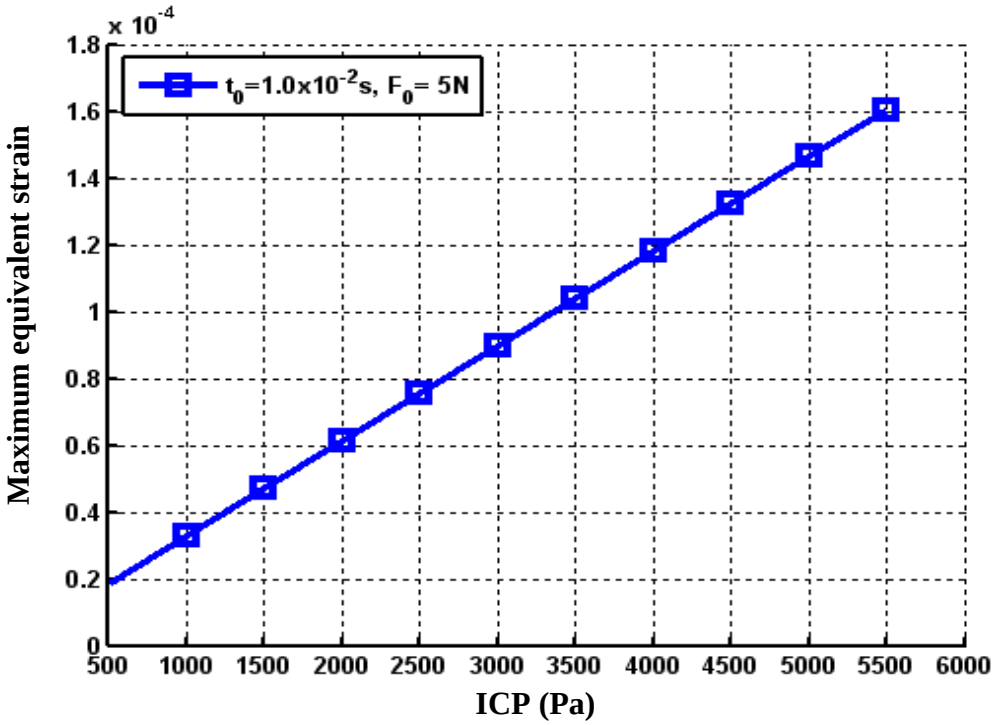

Figure 3.3 (d): Correlation between ICP and $\varepsilon_e^{\max}$

From Figure 3.3, it can be observed that a strong correlation does exist between ICP and each vibration response. The correlation curves are approximately linear. That is, ICP has approximately linear relationship with the maximum displacement ($u_x^{\max}$), maximum velocity ($v_x^{\max}$), maximum acceleration ($a_x^{\max}$) and maximum equivalent strain ($\varepsilon_e^{\max}$).

The correlation curves show that as ICP increases, all the vibration response increase. Another observation is that, for each vibration response, there is no obvious distinction between correlation curves in the normal ICP range (from 500Pa to 2000Pa) and that in the abnormal ICP range (larger than 2000Pa). These correlations are very useful for determining ICP. Once a response is collected, extract its maximum value, and then the ICP can be easily obtained from the corresponding correlation curve. This indicates that evaluating ICP by virtue of a correlation between ICP and a vibration response is feasible.

3.2 Effects of impact magnitude

In this section, three impact magnitudes are used to study its effect on the correlations between ICP and external vibration responses. The studied impact magnitudes are 1 N, 5 N and 10 N. For each impact magnitude, a set of solutions and post-processings with the eleven selected ICPs were carried out. Among the three sets FE analyses, impact magnitude is the only difference. The impact duration is 10 ms in this study. The procedure of conducting each FE analysis is the same as that described in Section 3.1.

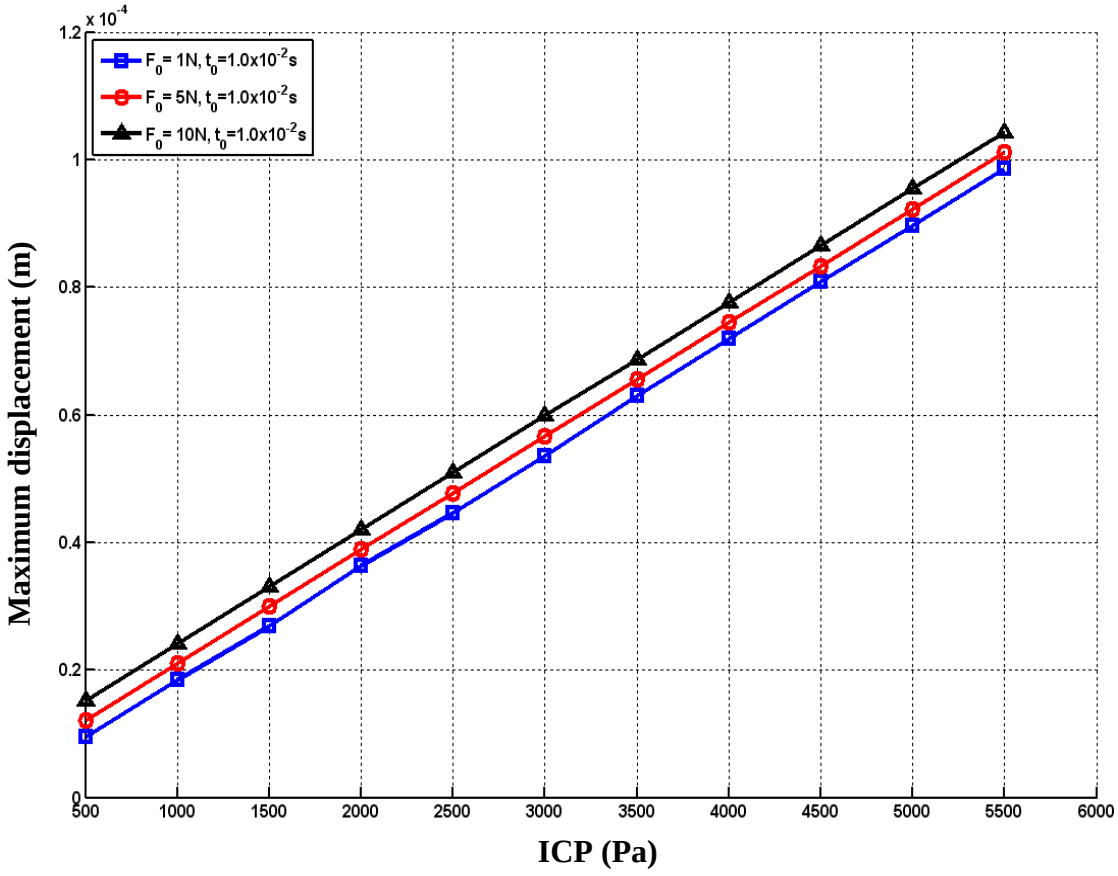

Figure 3.4: Correlation between ICP and u_x^{max} for F_0=1 N, F_0=5 N and F_0=10 N, respectively

3.2 Effects of impact magnitude

Figure 3.4 displays the correlation between ICP and displacement for F_0=1 N, F_0=5 N and F_0=10 N, respectively. It can be seen that the three correlation curves are all approximately linear. The slopes are all 1.76 $\times 10^{-8}$ m/Pa. Maximum displacement u_x^{max} increases as ICP goes up. The impact magnitude does not change the correlation pattern between ICP and the maximum displacement u_x^{max}.

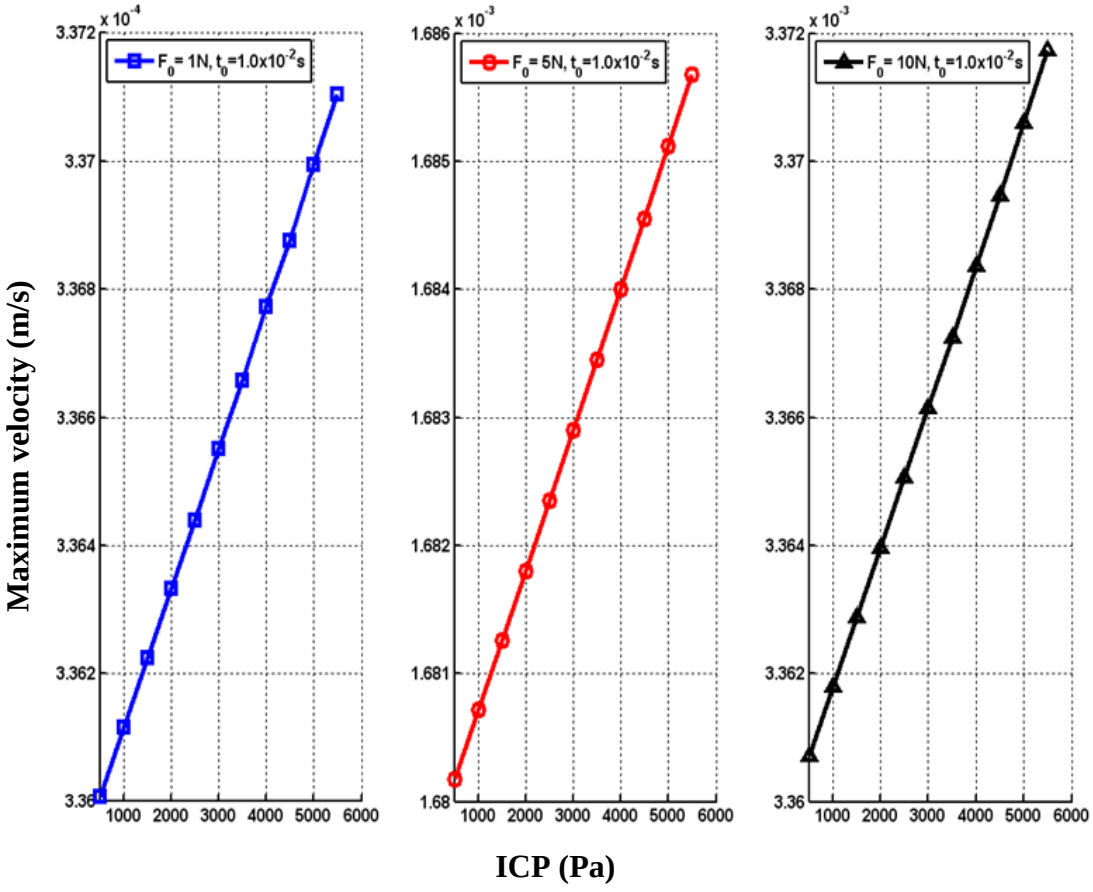

Figure 3.5: Correlation between ICP and v_x^{max} for
F_0=1 N, F_0=5 N and F_0=10 N, respectively

3.2 Effects of impact magnitude

The correlation between ICP and maximum velocity is shown in Figure 3.5. For one impact magnitude (e.g., F_0=1 N), the change of the maximum velocity Δv_x^{max} (from ICP = 500 Pa to ICP = 5500 Pa) is: (3.3712 - 3.3600) $\times 10^{-4}$ m/s = 1.12×10^{-6} m/s. so the change of the maximum velocity Δv_x^{max} is very small in comparison to the maximum velocity v_x^{max}, i.e., 1.12×10^{-6} m/s vs. 3.3712 $\times 10^{-4}$ m/s. For F_0 = 5 N, Δv_x^{max} vs. v_x^{max} = 5.6 $\times10^{-6}$ m/s vs. 1.6858 $\times10^{-3}$ m/s, and for F_0=10 N, Δv_x^{max} vs. v_x^{max} = 1.16 $\times10^{-5}$ m/s vs. 3.3719 $\times10^{-3}$ m/s. If the three correlation curves are plotted in one graph, the three correlation curves are look like parallel to each other, and the maximum velocity changes as ICP increases can hardly be seen. So three graphs are employed here to ensure the changes of the correlation curves can be clearly displayed. One observation is that maximum velocity v_x^{max} increases as ICP rises.

3.2 Effects of impact magnitude

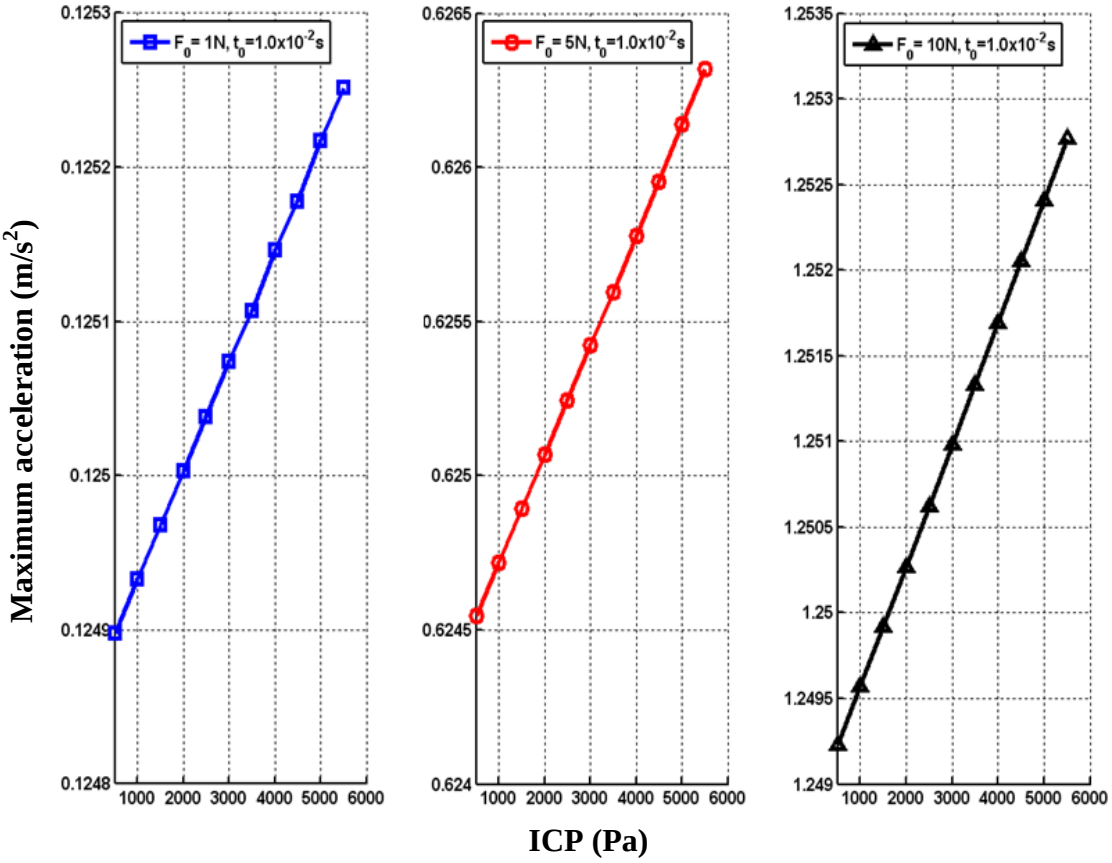

Figure 3.6: Correlation between ICP and a_x^{max} for F_0=1 N, F_0=5 N and F_0=10 N, respectively

Correlations between ICP and maximum acceleration a_x^{max} obtained by the three impact magnitudes are displayed in Figure 3.6. Same to maximum velocity, the change of the maximum acceleration Δa_x^{max} (from ICP = 500 Pa to ICP = 5500 Pa) is very small compare to the maximum acceleration a_x^{max}. For F_0= 1 N, Δa_x^{max} vs. a_x^{max} = 3.6 $\times 10^{-4}$ m/s^2 vs. 0.12526 m/s^2; for F_0= 5 N, Δa_x^{max} vs. a_x^{max} = 1.95 $\times 10^{-3}$ m/s^2 vs. 0.62546 m/s^2; for F_0 =10 N, Δa_x^{max} vs. a_x^{max} = 3.5 $\times 10^{-3}$ m/s^2 vs. 1.2527 m/s^2. Thus, the three correlation curves are plotted in three graphs. It can be seen from Fig. 3.6 that maximum acceleration increases as ICP goes up.

3.2 Effects of impact magnitude

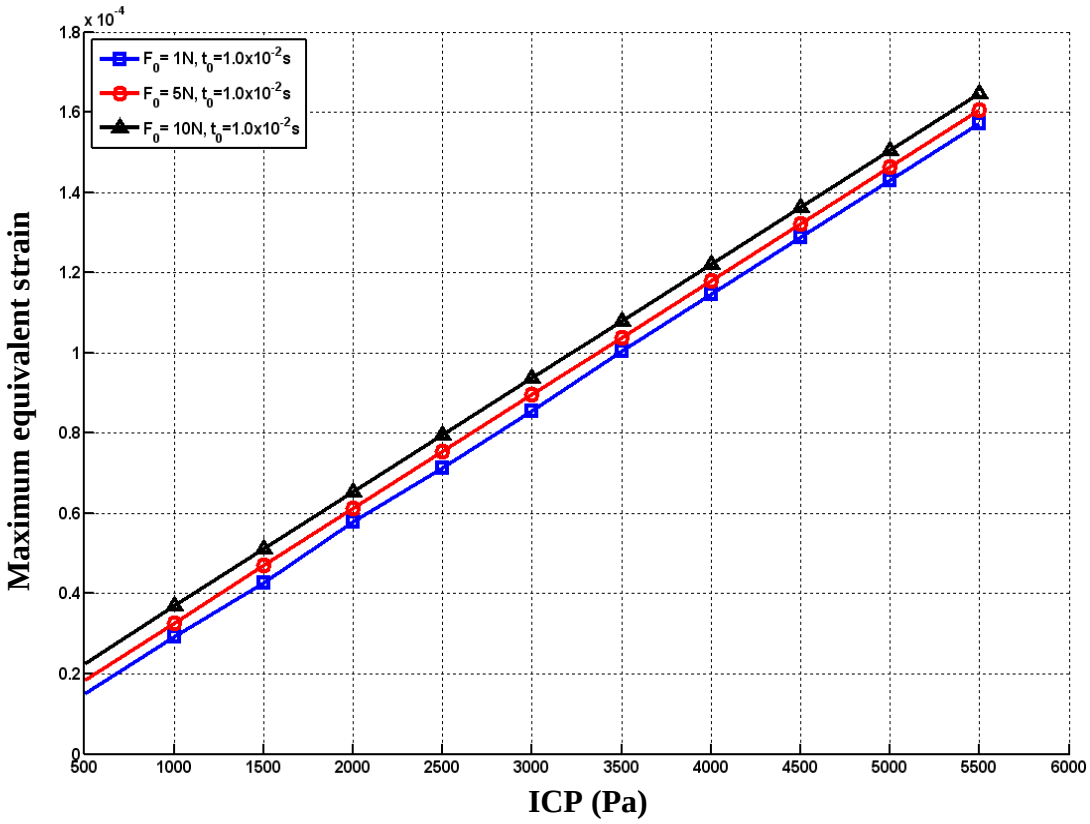

Figure 3.7: Correlation between ICP and $\varepsilon_e^{\max}$ for F_0=1 N, F_0=5 N and F_0=10 N, respectively

The corresponding correlations between ICP and maximum equivalent strain are shown in Figure 3.7. It can be seen that the three correlation curves are all approximately linear. Maximum equivalent strain $\varepsilon_e^{\max}$ increases as ICP goes up. The impact magnitude does not change the correlation pattern between ICP and the maximum equivalent strain $\varepsilon_e^{\max}$.

From the above study, it can be concluded that change in impact magnitude does not affect the correlation patterns between ICP and the studied vibration responses for F_0=1 N, F_0=5 N and F_0=10 N. However, the maximum magnitudes of the vibration responses do change with impact magnitude. The study in this section is very useful for ICP deter-

mination in practice. The smaller the applied impact, the less painful the patient is. Without influencing the accuracy of ICP's determination, the impact magnitude should be as small as possible. Although the minimum impact magnitude used in the study is 1 N, smaller magnitude is still possible depending on the sensitivity of the transducer installed at location B which is shown in Figure 3.1. For instance, if the correlation between ICP and maximum displacement are used in the afterwards proposed procedure for evaluating ICP, the collected maximum displacement for ICP = 500 Pa is 0.12×10^{-4} m, i.e., 12 μm, a sub-miniature linear gauge with nano resolution (for measuring displacement under 500 μm) can be used to measure the displacement.

3.3 Effects of impact duration

The effect of impact duration on the correlations between ICP and external vibration responses was investigated by three sets of FE analyses in this section. The impact duration is the only difference among the three sets of FE analyses. The durations are 10 ms, 1.0 ms and 0.1 ms, respectively. The same FE analysis procedure as in Sections 3.1 and 3.2 was used in the investigation, and the impact magnitude is 5 N.

3.3 Effects of impact duration

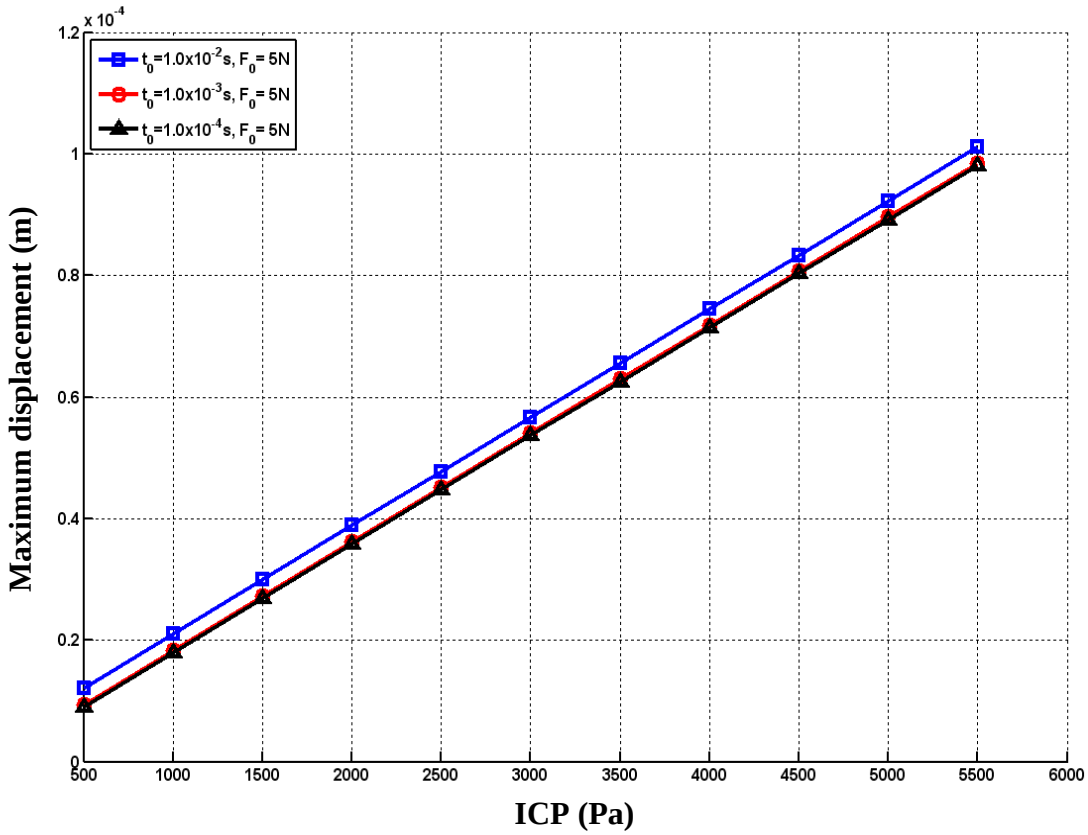

Figure 3.8: Correlation between ICP and u_x^{max} for
$t_0=1.0\times10^{-2}$ s, $t_0=1.0\times10^{-3}$ s and $t_0=1.0\times10^{-4}$ s, respectively

It can be observed from Figure 3.8 that the correlation pattern between ICP and maximum displacement is not affected by impact duration. The slopes of the three curves are all 1.78×10^{-8} m/Pa. For all the three durations, maximum displacement increases as ICP rises. For a particular ICP, longer duration generates larger maximum displacement, as more mechanical energy is input or applied to the head.

3.3 Effects of impact duration

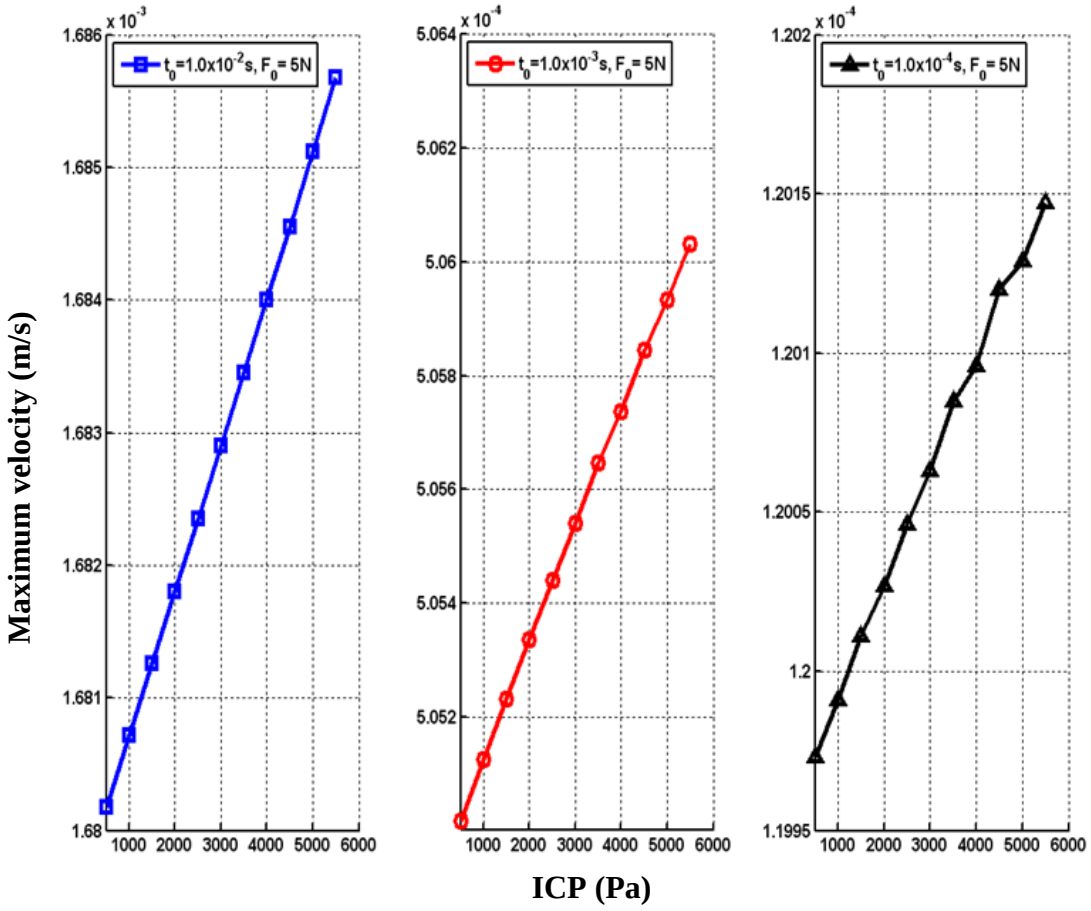

Figure 3.9: Correlation between ICP and v_x^{max} for $t_0=1.0\times10^{-2}$ s, $t_0=1.0\times10^{-3}$ s and $t_0=1.0\times10^{-4}$ s, respectively

From Figure 3.9, it can be seen that some differences exist between the three correlation curves. Correlation curves for t_0=10 ms and t_0=1.0 ms are approximately linear while the correlation curve for t_0=0.1 ms is less linear. Long duration generates larger maximum velocity for a particular ICP than short duration does. E.g. when ICP = 1000 Pa, the maximum velocity is 1.681×10^{-3} m/s, 5.050×10^{-4} m/s and 1.1997×10^{-4} m/s for t_0=10 ms, t_0=1.0 ms and t_0=0.1 ms, respectively. One phenomenon that is in common with dis-

placement vs. ICP correlations is that velocity ascends as ICP rises in all the three correlation curves.

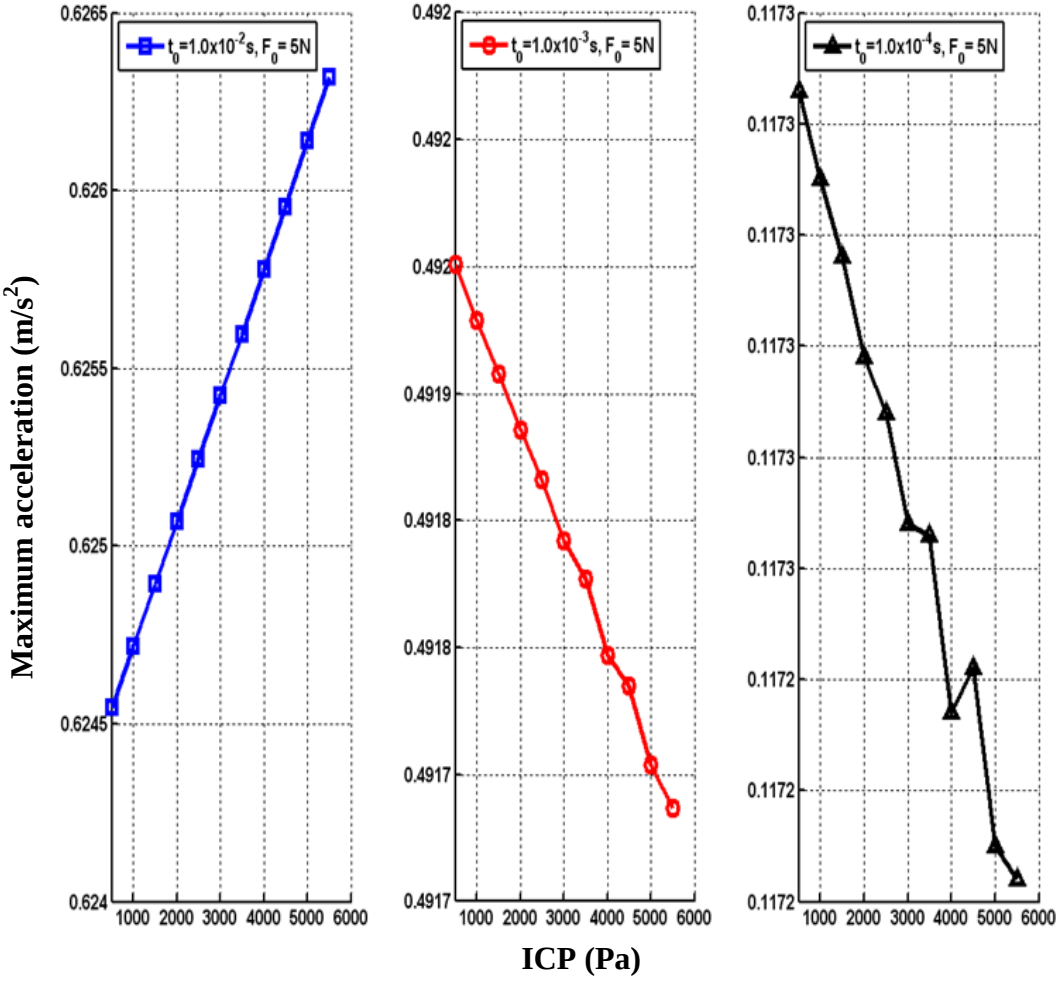

Figure 3.10: Correlation between ICP and a_x^{max} for $t_0=1.0\times10^{-2}$ s, $t_0=1.0\times10^{-3}$ s and $t_0=1.0\times10^{-4}$ s, respectively

Figure 3.10 displays the three correlation curves of maximum acceleration and ICP. They differ from each other considerably. Acceleration only goes up with ICP for t_0=10 ms, and the curve is approximately linear, while the correlation curves for t_0=1 ms and t_0=0.1 ms are less linear. Therefore, ICP vs. acceleration correlation patterns are different for different impact durations. One possible cause for the difference is the wave propaga-

tion. The wave propagates in the combination of reflection, refraction, diffraction and interference in human head. Impact duration influences the vibration of human head and further influences the dominant wave propagation. If impact duration larger than a certain time T_a, and reflection becomes the dominant propagation, the maximum acceleration decreases as ICP increases. Otherwise, maximum acceleration increases as ICP goes up. From Fig.3.10, T_a may larger than 1ms, and acceleration decreases when impact duration t_0=1 ms and t_0=0.1 ms.

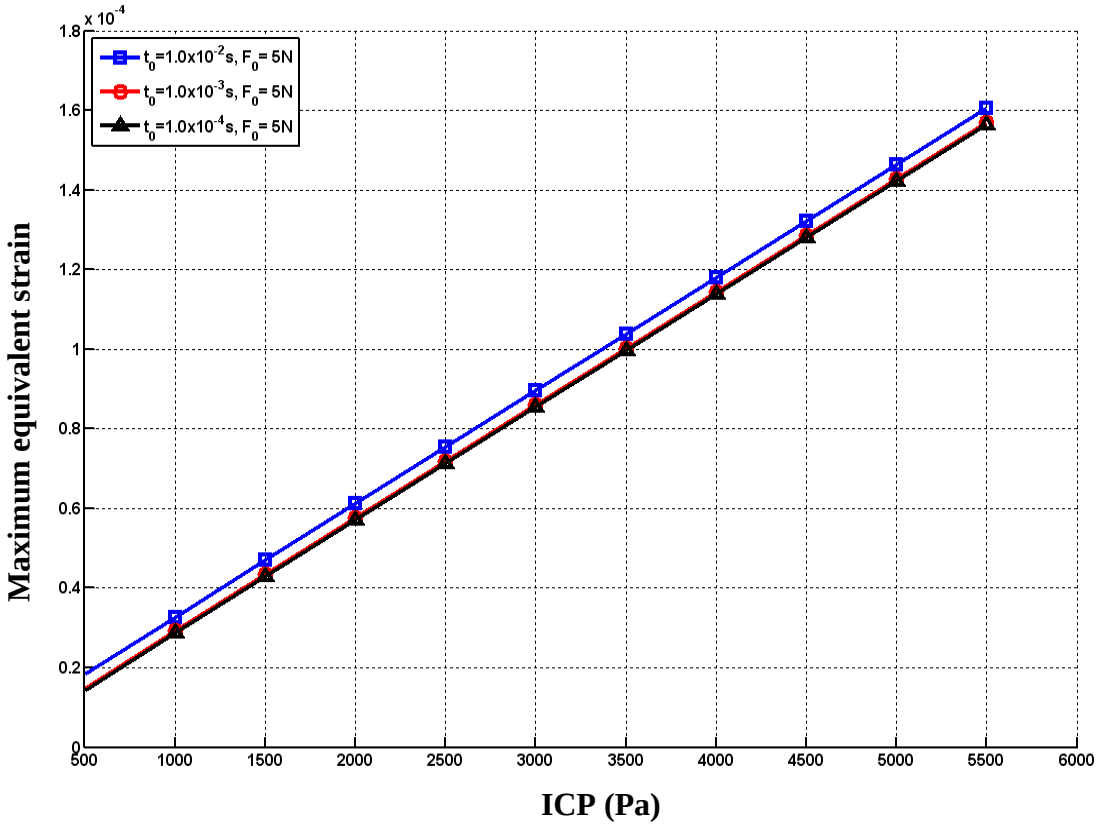

Figure 3.11: Correlation between ICP and ε_e^{max} for t_0=1.0 ×10^{-2} s, t_0=1.0 ×10^{-3} s and t_0=1.0 ×10^{-4} s, respectively

3.3 Effects of impact duration

From the correlations between ICP and maximum equivalent strain displayed in Fig. 3.11, it can be seen that correlations established by using different impact durations are similar to each other. The maximum equivalent strain goes up when ICP increases. Obviously, longer duration leads to larger maximum equivalent strain.

The impact duration show less effect on the correlation between ICP and maximum displacement, or maximum equivalent strain than on that for maximum velocity or maximum acceleration. For velocity and acceleration, a long impact duration produces more consistent and clear correlation than a short duration does. The obtained results indicate that impact duration shorter than a certain time is not good for establishing strong correlation between ICP and velocity, and correlation between ICP and acceleration.

Chapter 4

ICP Evaluation for CHI Patients

Based on the correlations established in Chapter 3, a non-invasive procedure for evaluating ICP of CHI patients is developed in this chapter. In order to select the most appropriate vibration response to evaluate ICP, the sensitivity of vibration response to ICP change will be introduced. The four vibration responses will be studied and compared with respect to their sensitivities. Based on the comparison, a vibration response will be selected for establishing a procedure for evaluating ICP of CHI patients.

4.1 Sensitivities of vibration responses to ICP change

In practice, it is desired that even a small change in ICP can be captured by a vibration response [70, 81]. It requires that the vibration response is sensitive to ICP changes. To evaluate the sensitivity of a vibration response to ICP changes, the following sensitivity definition is introduced.

4.1 Sensitivities of vibration responses to ICP change

$$\psi = \frac{\Delta\omega/\omega_a}{\Delta P/P_a} = \frac{\Delta\omega}{\Delta P} \times \frac{P_a}{\omega_a} = \frac{(\omega_u - \omega_l)}{(P_u - P_l)} \times \frac{P_a}{\omega_a} \tag{4.1}$$

Where ψ is the sensitivity; ω represents a vibration response; P is the intracranial pressure; $\Delta\omega$ and ΔP denote increments in the vibration response and in the intracranial pressure, respectively. To eliminate the units of $\Delta\omega$ and ΔP, a normalization is used, that is introducing P_a and ω_a in the formula 4.1. For each increment, ω_a is the average value of a vibration response; while P_a is the average ICP. Subscripts u and l stand for the upper and lower values of an increment in ICP or in the vibration response, respectively. ω_u and ω_l are the maximum responses for the upper and lower ICP in an increment, respectively. ψ, reflects the relative change of the vibration response with respect to an ICP change.

Table 4.1: Sensitivities of the four vibration responses to ICP change

ICP	$u_x^{\max}$	$v_x^{\max}$	$a_x^{\max}$	$\varepsilon_e^{\max}$
500~1000	0.9459	0.0010	0.0017	0.9548
1000~1500	0.9452	0.0010	0.0017	0.9541
1500~2000	0.9445	0.0010	0.0017	0.9534
2000~2500	0.9438	0.0010	0.0017	0.9528
2500~3000	0.9431	0.0010	0.0017	0.9521
3000~3500	0.9424	0.0010	0.0017	0.9514
3500~4000	0.9417	0.0010	0.0017	0.9508
4000~4500	0.9409	0.0010	0.0017	0.9500
4500~5000	0.9402	0.0010	0.0017	0.9494
5000~5500	0.9395	0.0010	0.0017	0.9487
Averaged	0.9427	0.0010	0.0017	0.9517

Table 4.1 lists the sensitivities of the vibration responses for impact magnitude F_0 = 5 N and duration t_0 =10 ms. The averaged sensitivity of maximum displacement, velocity, acceleration and equivalent strain are 0.9427, 0.0010, 0.0017 and 0.9517, respectively. That is, the maximum displacement and maximum equivalent strain are more sensitive to ICP change than maximum velocity and maximum acceleration. Based on the above study, both the ICP vs. displacement correlation and ICP vs. equivalent strain correlation can be used for ICP evaluation and a procedure for evaluating ICP is proposed in the following section.

4.2 Patient specific procedure for evaluating ICP

Steps of a proposed non-invasive procedure for evaluating ICP are illustrated in Figure 4.5 [81]. STEP 1: Establishment of a patient-specific correlation between ICP and a vibration response. The procedure starts with getting a medical image of the patient's head, e.g., take a MR image. A geometric model is constructed from the medical image of the patient by using a software, e.g., MATLAB. Based on the geometric model, a patient-specific FE model of the human head is built and FE analyses are then conducted. Correlation between ICP and a vibration response, e.g. maximum displacement, is established using the method described in Chapter 3. Figure 4.1 shows the steps of establishing the patient-specific correlation between ICP and a vibration response.

4.2 Patient specific procedure for evaluating ICP

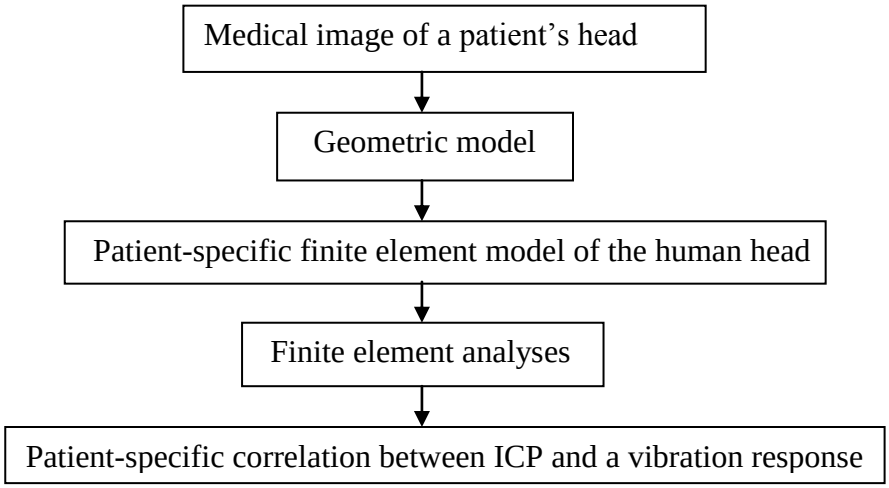

Figure 4.1: Establishment of a patient-specific correlation between ICP and a vibration response

STEP 2: Instrument setup. A device with two transducers is attached onto the patient's head using an elastic band. Installation of the device is shown in Figure 4.2. The transducer installed at location **A** is used for generating a harmless impact (e.g., a step impulse) and the transducer installed at location **B** is used for picking up vibration responses. One attention should be paid here is that the location for applying the step impulse and picking up the vibration responses should be the same to those in the FE method.

STEP 3: Computer operation. Under the control of a computer, transducer **A** generates an impulse. Since a vibration response is related to the duration and magnitude of the impact that are discussed in the previous chapter, the duration and magnitude of the impact applied in practice should be consistent with those applied in the FE method. That is, if the impulse is a step impulse with duration of 10 ms and a magnitude of 5 N used in the

FE method, these values should be the same in practice. Transducer **B** picks up a vibration response, e.g., displacement, and sends them to the computer. The maximum displacement is then extracted by a computational algorithm.

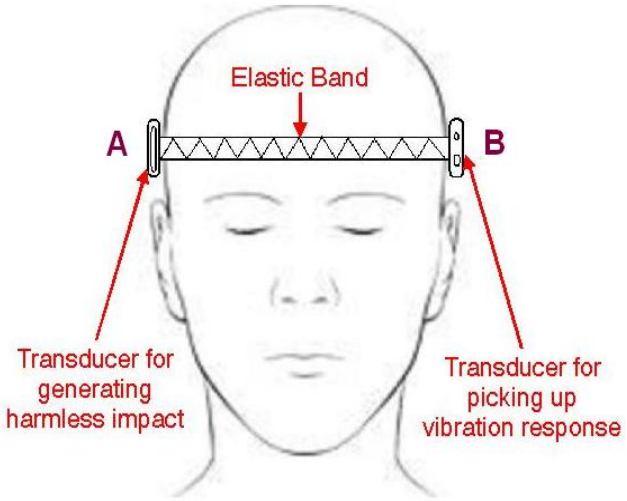

Figure 4.2: Instrument setup for measuring ICP

STEP 4: ICP evaluation. Based on the correlation between ICP and maximum displacement established by FE analyses in STEP1, the ICP of the patient can be determined from the maximum displacement measured in STEP 3. An example of three possible outcomes from the proposed procedure is shown in Figure 4.3.

4.2 Patient specific procedure for evaluating ICP

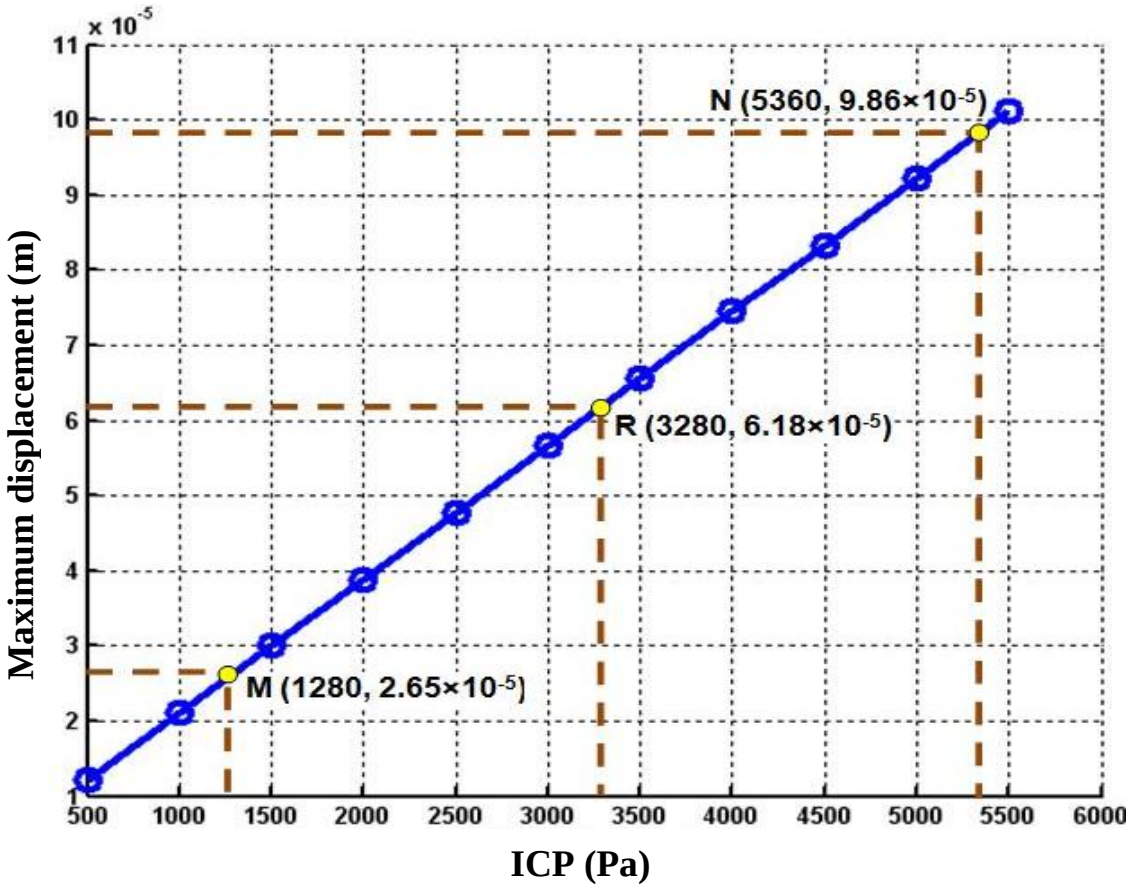

Figure 4.3: Three possible outcomes in ICP evaluation

In the first scenario (marked by M in the figure), the measured maximum displacement is 2.65×10^{-5} m, the ICP determined by the correlation is 1280 Pa. In the second scenario (indicated by R), the measured maximum displacement is 6.18×10^{-5} m, the corresponding ICP obtained from the correlation is 3280 Pa. In the third case (represented by N), the measured maximum displacement is 9.86×10^{-5} m, and the determined ICP is 5360 Pa. Based on reported studies [12, 21, 24], the normal range of ICP is between 3.75 mmHg and 15 mmHg, or between 500 Pa ~ 2000 Pa. ICP above 20 mmHg (2666 Pa) is considered abnormally high and ICP greater than 40 mmHg (5333 Pa) is a severe condition [6, 12, 24]. If ICP exceeds 45 mmHg (6000 Pa), the patient is in a fatal condition.

4.2 Patient specific procedure for evaluating ICP

Based on the above classification, in scenario M, the person is in a normal condition. In scenario R, the patient's ICP is abnormally high, and an immediate treatment should be taken. While in scenario N, the patient is in a critical condition and an emergent surgery is required.

Chapter 5

Conclusions and Future Work

5.1 Conclusions

Since ICP is a significant parameter that reflects CHI patient's severity and physiological state, many methods have been developed to evaluate and monitor ICP. Existing methods for evaluating ICP were evaluated and compared. Invasive methods may bring infection and haemorrhage, while existing non-invasive methods are not reliable for measuring absolute ICP.

Results obtained from the FE study showed that strong correlations do exist between ICP and vibration responses. The results on the effect of impact magnitude indicated that larger magnitude leads to greater vibration responses, and the magnitude does not influence the correlation patterns between ICP and the four external vibration responses (i.e., displacement, velocity, acceleration and equivalent strain) for the studied impact magnitudes which are 1 N, 5 N and 10 N. The impact duration which are 10 ms, 1 ms and 0.1 ms affect different vibration responses differently. The ICP vs. acceleration correlation

pattern is affected by impact duration obviously, while the impact duration affects that of ICP vs. velocity to some extent. However, the impact duration has very little effect on the correlation patterns of ICP vs. displacement and ICP vs. equivalent strain.

Response sensitivity was introduced to measure how sensitive a vibration response is to an ICP change. It was found that displacement and equivalent strain are more sensitive than velocity and acceleration to ICP. This is consistent with the observations from time histories of the four responses. Based on the studied results, a procedure was proposed for ICP evaluation.

5.2 Future work

The research reported in this thesis is preliminary. Further research needs to be done before the proposed non-invasive procedure can be implemented as a medical instrument and applied in clinics:

1. *Building a more complicated 2D finite element model:* The human head has a complex geometry that has not accurately represented by the 2D FE model in this thesis. Therefore, a 2D FE model with more intracranial constituents will be constructed by following the same process as used for constructing the model in this thesis. Considering the materials of some intracranial components as heterogeneous is also a further work for 2D modeling.
2. *Establishing a realistic 3D finite element model*. If the correlation between ICP and external vibration responses for the more complicated 2D FE model is also strong, a 3D FE model of human head will be established. With the 3D FE model

of human head, it is possible to predict the realistic responses of the human head to loading impacts.

3. *Design of a medical instrument*: A medical instrument satisfies the requirement described in the proposed procedure in Section 4.2 will be designed. A filter will be included in the instrument to eliminate or reduce the environment noise and some other interference noise. If the external response signal of the vibration excited by the loading impact has similar amplitude to that of noise signal, a larger loading impact will be considered. The prerequisite is that the impact is harmless to human head. More details on the specifications of the transducers are needed to be figured out.
4. *Experiment validation and verification of 3D FE model*: The correlations established by the 3D FE model will be validated by an invasive method. The medical instrument designed in the above will be used to collect vibration responses from the patient, and the ICP obtained from the proposed non-invasive procedure will be compared with that from the invasive method.

Bibliography

[1] G.Critchley and A.Memon. Epidemiology of head injury. In P.C.Whitfield, E.O.Thomas, F.Summers, M.Whyte, and P.J.Hutchinson, editors, *Head Injury: A Multidisciplinary Approach*. Cambridge University Press, 2009.

[2] D. Kushner. Mild traumatic brain injury: Toward understanding manifestations and treatment. *Archives of Internal Medicine*, 158:1617 – 1624, 1998.

[3] S. McDonald, L. Togher, and C. Code. *Communication Disorders Following Traumatic Brain Injury*. Psychology Press, 1st edition, 1999.

[4] Y. Luo, Q. Zhang, and M. Del Bigio. Recent progress in application of finite element method in study of non-penetrating brain injuries. *Advances in Theoretical and Applied Mechanics*, 1:225 – 240, 2008.

[5] S.Gong, H. Lee, and C. Lu. Dynamic response of a human head to a foreign object impact. *IEEE Transactions on Biomedical Engineering*, 55:1226 – 1229, 2008.

[6] Z. Li, Y. Luo, H.Chen, Q. Zhang, and M.Del Bigio. On evaluation of intracranial pressure in closed head injury. *International Journal for Multiscale Materials Modeling*, Vol. 1, 9-23, 2010.

[7] E. S. Gurdjian, J. E. Webster, and H. R. Lissner. Mechanism of scalp and skull injuries, concussion, contusion and laceration. *Journal of Neurosurgery*, 15(2):125 – 128, 1958.

[8] E.S. Gurdjian, B. Audet, R.w. Sibayan, and L.M. Thomas. Spasm of the extracranial internal carotid artery resulting from blunt trauma demonstrated by angiography. *Journal of Neurosurgery*, 35:742 – 747, 1971.

[9] S. Parikh, M. Koch, and R. K. Narayan. Traumatic brain injury. *International Anesthesiology Clinics*, 45(2):119 – 135, 2007.

[10] R.A.Weerakkody, M. Czosnyka, R.A.Trivedi, and P.J.Hutchinson. Intracranial pressure monitoring in head injury. In P.C.Whitfield, E.O.Thomas, F.Summers, M.Whyte, and P.J.Hutchinson, editors, *Head Injury: A Multidisciplinary Approach*. Cambridge University Press, 2009.

[11] S. Milan, R.W. George, D.B. Joe, P.G. George, S.F. Kirk, C.L. Gary, A.T. Willis, and C. Allen. The effect of elevated intracranial pressure on the vibrational response of the ovine head. *Annals of Biomedical Engineering*, 23:720 – 727, 1995.

[12] E. Paraicz. ICP in infancy and childhood. *Monographs in paediatrics*, 15:1 – 7, 1982.

[13] A.W. Teresa, R.W. George, T.M. Mark, and D.B. Joe. Measurement and Modeling of the vibrational response of the ovine head as it relates to the intracranial pressure. In

18th Annual International Conference of the IEEE Engineering in Medicine and Biology Society, Amsterdam, Netherlands, October 31-November 3 1996.

[14] B.Mokri. The monro-kellie hypothesis: Applications in cerebrospinal fluid volume depletion. *Neurology*, 56(12):1746 – 1748, 2001.

[15] M.D. Gilchrist and D.O. Donoghue. Simulation of the development of frontal head impact injury. computational mechanics. *Computational Mechanics*, 26:229 – 235, 2000.

[16] G. Dassios, M.K. Kiriakopoulos, and V. Kostopoulos. On the sensitivity of the vibrational response of the human head. *Computational Mechanics*, 21:382–388, 1998.

[17] J.H.McElhaney, V.L.Roberts, and J.F.Hilyard. *In Handbook of Human Tolerance*. Japan Automobile Research Institute, Inc., 1976.

[18] G.Teasdale and D.Mendelow. Pathophysiology of head injuries. In N.Brooks, editor, *Closed Head Injury: Psychological, Social, and Family Consequences*. Oxford University Press, 1984.

[19] J.M. John and P.W. Arthur. *Critical Care Medicine: the Essentials*. Lippincott Williams & Wilkins, 3rd edition, 2006.

[20] R. Allen. Intracranial pressure: a review of clinical problems, measurement techniques and monitoring methods. *Journal of Medical Engineering & Technology*, 10:299 – 320, 1986.

[21] J. Ghajar. Intracranial pressure monitoring techniques. *New Horizons*, 3:395 – 399, 1995.

[22] E.C. Mick and N.H. Chester. Method and apparatus for the measurement of intracranial pressure. *US Patent 5117835*, 1992.

[23] H.H. Merrit and S.F. Fremont. The cerebrospinal fluid. *US Patent, Philadelphia*, 1937.

[24] R.A. Minns. Intracranial pressure monitoring. *Archives of Disease in Childhood*, 59:486 – 488, 1984.

[25] M. Czosnyka and J. D. Pickard. Monitoring and interpretation of intracranial pressure. *Neuroscience for Neurologists*, 75:813 – 821, 2004.

[26] L.A. Steiner and P.J.D. Andrews. Monitoring the injured brain: ICP and CBF. *British Journal of Anaesthesia*, 97:26–38, 2006.

[27] P.H. Chapman, E.R. Cosman, and M.A. Arnold. The relationship between ventricular fluid pressure and body position in normal subjects and subjects with shunts: a telemetric study. *Neurosurgery*, 26:181–189, 1990.

[28] A. Hulme and R.Cooper. The effects of head position and jugular vein compression (JVC) on intracranial pressure (ICP), a clinical study. *Intracranial Pressure III*, pages 259–263, 1976.

[29] H.M. Shapiroh. Intracranial hypertension: therapeutic and anesthetic considerations. *Anaesthesiology*, 43:445–471, 1975.

[30] D.N. Sinha. Method for non-invasive intracranial pressure measurement. *US Patent 6117089*, 2000.

[31] G. Jamshid. Traumatic brain injury. *The Lancet*, 356:923 – 929, 2000.

[32] K.Omori, L. Zhang, K.H. Yang, and A.I. King. Effect of ceerebral vasculatures on the mechanical response of brain tissue: a preliminary study. In *Symposium on Crashworthiness, Occupant Protection and Biomechanics in Transportation Systems*, volume 246, pages 167 – 174, New York, USA, 2000.

[33] M. Beek, J. Koolstra, L.V. Ruijven, and T. V. Eijden. Three-dimensional finite element analysis of the human temporomandibular joint disc. *Journal of Biomechanics*, 33:307 – 316, 2000.

[34] D. Bouattoura, P. Gaillard, P. Villon, and F. Langevin. Brain evoked potential topographic mapping based on the diffuse approximation. *Medical & Biological Engineering & Computing*, 36:415 – 421, 1998.

[35] E. Johnson and P. Young. On the use of a patient-specific rapid-prototyped model to simulate the response of the human head to impact and comparison with analytical and finite element models. *Journal of Biomechanics*, 38:39 – 45, 2005.

[36] R. Lapeer and R. Prager. 3D shape recovery of a newborn skull using thin-platesplines. *Computerized Medical Imaging and Graphics*, 24:193 – 204, 2000.

[37] B. V. Mehta and S. Rajani. 3D Modeling and analysis of human bones: generating 3D models to accommodate varying material properties for finite element analysis. *American Society of Mechanical Engineers*, 77:117 – 125, 1996.

[38] N.F. kostas, S. Arturas, E.C. Troup, H.F. Carlos, D. Vasilios, D. Vytenis, G. Daubaris, A. Ragauskas, and S.R.J. Joe. New non-invasive sonographic modality for intracranial pressure/volume monitoring. *Child's Nerve System*, 18:211 – 214, 2002.

[39] C.M. Robert and B.P.S. John. Rapid bedside technique for intracranial pressure monitoring. *The Lancet*, 324:73 – 75, 1984.

[40] H.K. Marin, J.B. Timpthy, and I. Warren. *The Washington manual of critical care*. Lippincott Williams & Wilkins, 2007.

[41] J.K. Vries, D.P. Becker, and H.F. Young. A subarachnoid screw for monitoring intracranial pressure. *Journal of Neurosurgery*, 39:416 – 419, 1973.

[42] J.J.F. Perkins. *The Relation of the Cerebrospinal Fluid to Respiration: a Brief Historical Introduction*. Blackwell Scientific Publications, Oxford, 1965.

[43] S.V. Ahmed, C. Jayawarna, and E.Jude. Post lumbar puncture headache: diagnosis and management. *Postgraduate Medical Journal*, 82:713–716, 2006.

[44] R. Grant, B. Condon, I. Hart, and G.M. Teasdale. Changes in intracranial CSF volume after lumbar puncture and their relationship to post-LP headache. *Journal of Neurology, Neurosurgery, and Psychiatry*, 54:440 – 442, 1991.

[45] D. Vidyasagar and T.N.K. Raju. A simple noninvasive technique of measuring intracranial pressure in the newborn. *Pediatrics*, 59:957–961, 1977.

[46] D. Vidyasagar. Intracranial pressure monitoring as an adjunct to the management of sick neonates. In S. Kumar and M. Rathi, editors, *Perinatal Medicine*, pages 151–163. Pergamon Press, Oxford, 1977.

[47] J.A. Allocca. Method and apparatus for non-invasive monitoring of intracranial pressure. *US Patent 4204547*, 1980.

[48] N. Alperin. Method of measuring intracranial pressure. *US Patent 5993398*, 1999.

[49] M.S. Borchert and J.L. Lambert. Non-invasive method of measuring cerebral spinal fluid pressure. *US Patent 6129682*, 2000.

[50] K. Bridger, A.V. Cooke, F.j. Crowne, P.M. Kuhn, and J.J. Lutian. Apparatus and method for measurement of intracranial pressure with lower frequencies of acoustic signal. *US Patent 5919144*, 1999.

[51] J.R.Madsen and G.A. Taylor. Non-invasive in vivo pressure measurement. *US Patent 6086533*, 2000.

[52] N. Kageyama and N. Sakuma. Apparatus for recording intracranial pressure. *US Patent 4971061*, 1990.

[53] N. Kageyama and N. Sakuma et al. Apparatus for measuring intracranial pressure. *US Patent 4984567*, 1991.

[54] D. Michaeli. Ultrasound apparatus and method for tissue resonance analysis. *US Patent 6702743*, 2003.

[55] P.D. Mourad and M.Kliot et al. Systems and methods for making noninvasive physiological assessments. *US Patent 6875176*, 2002.

[56] A. Ragauskas, G. Daubaris, S.Rocka, and V. Petkus. Innovative technologies of head injury physiological monitoring. *Ultragarsas*, 4:51–57, 2000.

[57] A. Ragauskas, G. Daubaris, V. Petkus, R. Raisutis, R. Chomskis, R. Sliteris, V. Deksnys, J. Guzaitis, and G. Lengvinas. Non-invasive assessment of intracranial bio-mechanics of the human brain. *Ultragarsas*, 63.

[58] A. Ragauskas, G. Daubaris, V. Ragaisis, and V. Petkus. Implementation of non-invasive brain physiological monitoring concepts. *Medical Engineering and Physics*, 25:667 – 678, 2003.

[59] J.G. Rosenfeld, C. Watts, and D.H. York. Method and apparatus for intracranial pressure estimation. *US Patent 4564022*, 1986.

[60] W.T. Yost and J.J.H. Cantrell. Non-invasive method and apparatus for monitoring intracranial pressure and pressure volume index in human. *US Patent 5617873*, 1997.

[61] M.Stevanovic, G.R.Wodicka, J.D.Bourland, G.P.Graber, K.S.Foster, G.C.Lantz, W.A.Tacker, and A.Cymerman. The effect of elevated intracranial pressure on the vibrational response of the ovine head. *Annals of Biomedical Engineering*, 23:720–727, 1995.

[62] T.A.Whitman, G.R.Wodicka, M.T.Morgan, and J.D.Bourl. Measurement and modeling of the vibrational response of the ovine head as it relates to intracranial pressure. In *Ann.Int.Conf.of the IEEE Engineering in Medicine and Biology-proceedings*, volume 2, pages 493 – 494, Amsterdam, Neth, 1996.

[63] V.Kostopoulos, E.E.Douzinas, E.M.Kypriades, and Y.Z.Pappas. A new method for the early diagnosis of brain edema/brain swelling.an experimental study in rabbits. *Journal of Biomechanics*, 39:2958 – 2965, 2006.

[64] A.A.H.J.Sauren and M.H.A. Claessens. *Finite Element Modeling of Head Impact: the Second Decade*. International Research Council on Biomechanics of Injury, 1993.

[65] J.N.Reddy. *An Introduction to the Finite Element Method*. McGraw-Hill, 3rd edition, 2004.

[66] L.F. Squire and R.A. Noveline. *Squire's Fundamentals of Radiology*. Harvard University Press, 5th edition, 1997.

[67] L.Y.Cheng, S.Rifai, T.Khatua, and R.L.Piziali. Finite element analysis of diffuse axonal injury. In *Poc. 34th Stapp Car Crash Conf., SAE Paper 900547*, pages 141–154, 1990.

[68] D.Hutton. *Fundamentals of Finite Element Analysis*. McGraw-Hill, 1st edition, 2004.

[69] O.C. Zienkiewicz, R.L.Taylor, and J.Z.Zhu. *The Finite Element Method: Its Basis and Fundamentals*. Butterworth-Heinemann, Linacre House, Jordan Hill, 6th edition, 2005.

[70] Z. Li and Y. Luo. Finite element study of correlation between intracranial pressure and dynamic responses of human head. *Advances in Theoretical and Applied Mechanics*, 3(3):139 – 149, 2010.

[71] W. Goldsmith. The state of head injury biomechanics: past, present, and future: Part 1. *Critical Reviews in Biomedical Engineering*, 29:441 – 600, 2001.

[72] W. Goldsmith. The state of head injury biomechanics: past, present, and future. part 2: Physical experimentation. *Critical Reviews in Biomedical Engineering*, 33:105 – 207, 2005.

[73] O.C. Zienkiewicz, R.L.Taylor, and P. Nithiarasu. *The Finite Element Method for Fluid Dynamics*. Elsevier Butterworth-Heinemann, Amsterdam, Boston, 6th edition, 2005.

[74] E.Madenci and I.Guven. *The Finite Element Method and Applications in Engineering using ANSYS*. Springer Science + Business Media, LLC, 233 Spring street, New York, USA, 2006.

[75] N.M. Newmark. A method of computation for structural dynamics. *ASCE Journal of the Engineering Mechanics Division*, 85, 1959.

[76] E. L.Wilson. Dynamic response by step-by-step matrix analysis. *Proceedings, Symposium on the use of computers in civil engineering*, pages 1 – 5, 1962.

[77] ANSYS, Inc. Theory reference for ANSYS and ANSYS workbench, ANSYS 11.0 documentation. SAS IP, Inc., 2007.

[78] L.Voo, S.Kumaresan, F.A.Pintar abd N.Yoganandan, and A.Jr.Sances. Finite element models of the human head. *Medical & Biological Engineering &Computing*, 34:375 – 381, 1996.

[79] R.Willinger, H.S.Kang, and B.Diaw. Three-dimensional human head finite-element model validation against two experimental impacts. *Annals of Biomedical Engineering*, pages 403 – 410, 1999.

[80] C.C.Ward, M.Chan, and A.M.Nahum. Intracranial pressure - a brain injury criterion. In *Proceedings of the 24th Stapp Car Crash Conference, SAE Paper No. 80130*, pages 347–360, 1980.

[81] Z. Li and Y. Luo. Tentative non-invasive procedure for evaluating intracranial pressure. In *Proceedings of the Canadian Society for Mechanical Engineering Forum*, Victoria, BC, Canada, June 7 - June 9, 2010.